EcoScape: Species-specific Functional Habitat Connectivity Via Efficient Parallel Propagation Simulations

Natalia Ocampo-Peñuela*
nocampop@ucsc.edu
University of California
Santa Cruz, California, USA

Luca de Alfaro*
luca@ucsc.edu
University of California
Santa Cruz, California, USA

Jasmine Tai†
jasminecktai@gmail.com
Independent Contributor
California, USA

Natalie Valett†
natalievalett@gmail.com
Lund University
Sweden

Coen Adler†
ctadler@ucsc.edu
University of California
Irvine, California, USA

Artie Nazarov†
nazarov@hawaii.edu
University of Hawaiʻi
Mānoa, Hawaiʻi, USA

Montague H. C. Neate-Clegg
monteneateclegg@gmail.com
University of California
Davis, California, USA

July 2026

Abstract

Well-connected habitats sustain viable populations through gene flow, repopulation potential, and functional habitat extent. Conserving and enhancing habitat connectivity has been identified as a priority to halt extinctions and safeguard 30% of the planet. Conservation prioritization would therefore benefit from habitat connectivity modeling that is applicable at broad spatial and taxonomic scales. We introduce EcoScape, a species-specific computational tool capable of efficiently modeling habitat connectivity across large geographical areas. We describe how it estimates connectivity and flow relative to existing models. To evaluate its outputs, we map connectivity for three avian species across the contiguous United States, and we validate the resulting estimates against community-science occurrence data from eBird.

EcoScape performs hundreds of GPU-parallelized dispersal simulations seeded randomly in habitat, with propagation informed by each species' dispersal ability and habitat preferences. Connectivity is the probability that a habitat pixel can be repopulated from other habitat locations; flow is a pixel's contribution to downstream repopulation, highlighting matrix elements that facilitate connectivity. We demonstrate EcoScape on a synthetic landscape, then map both connectivity and flow layers for Acorn Woodpecker, Pileated Woodpecker, and Steller's Jay from Area of Habitat maps, habitat preferences, and dispersal abilities derived from a global trait dataset. We then use eBird checklists across each species' range to test whether connectivity predicts local occurrence and abundance after controlling for observer effort and habitat patch size.

In the synthetic landscape, we show how EcoScape predicts higher connectivity in larger and better-connected habitat patches, while flow between habitat is higher in a more permeable matrix. For the three focal species, we show that the computed connectivity positively predicts both local abundance and probability of occurrence in habitat grid cells beyond habitat patch size alone. We show that simulations can be efficiently performed in parallel on GPUs, leading to fast computation times that make it feasible to compute connectivity at continental scales.

EcoScape can be applied to any species with sufficient input data, is computationally efficient, and can be validated with readily available data. These advantages enable habitat connectivity mapping at large spatial scales and fine resolutions for hundreds of species, offering guidance for current and future conservation efforts.

Keywords

Dispersal ability, habitat conservation, landscape matrix, landscape permeability, habitat connectivity, model validation

1 Introduction

Habitat connectivity is essential for the long-term viability of animal and plant populations because it enhances species movement in the landscape, increasing the amount of functional habitat and ultimately maintaining genetic diversity [Taylor et al.(1993), Chase et al.(2020),

*Equal contribution
†The work was performed while the author was at the University of California, Santa Cruz, USA.

McRae and Beier(2007)]. Habitat protection and the maintenance of intact forest landscapes [Betts et al.(2017)] has long been recognized as a cornerstone of conservation [Watson et al.(2018), Brodie et al.(2025)]. In turn, habitat connectivity has become increasingly important in recent decades because it has the potential to mitigate the rampant impacts of habitat loss [Dickson et al.(2019), Olds et al.(2012)] and can enhance wildlife resilience to future environmental change [Heller and Zavaleta(2009)]. Furthermore, as climate change forces species to move upslope and latitudinally in search of suitable conditions, habitat connectivity is recognized as a principle conservation strategy to facilitate species adaptation in the face of climate change [Heller and Zavaleta(2009), McGuire et al.(2016), Littlefield et al.(2019)] .

As a result of this recognized need, global conservation frameworks have centered habitat connectivity within their goals. For example, the Convention on Biological Diversity (CBD) has set the goal of protecting 30% of the planet in "well-connected and equitably governed systems of protected areas and other effective area-based conservation measures" [Convention on Biological Diversity(2022)]. Spatial and predictive models can help the conservation community make informed decisions, allocate resources efficiently, and explore the outcomes of different conservation actions through scenario mapping [Beger et al.(2022), Zurell et al.(2025)]. For instance, identifying where to place new protected areas that conserve and enhance habitat connectivity would benefit from spatially explicit, multi-species, and regional-scale connectivity maps. To succeed in tackling this global challenge, habitat connectivity models ideally should: 1) rely on readily available input data; 2) be applicable to diverse taxa while considering inter-specific variability in their ecologies and how that affects relative connectivity; 3) be computationally efficient to enable scenario exploration, continental-scale coverage, and mapping for hundreds of species, and 4) be validated to increase reliability.

Habitat connectivity frameworks generally consider two facets of information that are useful for conservation decision making: habitat patch connectivity (accounting for both intra- and inter-patch dispersal [Spanowicz and Jaeger(2019)]) and the degree to which the matrix facilitates connectivity between habitat patches, i.e., matrix permeability. Habitat patch connectivity—where "habitat" is the primary breeding habitat of a species—refers to the extent to which a patch is linked to other patches in the landscape via dispersal [Hanski(1998)] and can serve to prioritize which existing habitat patches to conserve over others[Rayfield et al.(2011)]. For example, better-connected habitat patches could be the target of new protected areas [Simberloff and Abele(1982), Brennan et al.(2022)]. Matrix permeability—which focuses on the role of the matrix in landscape-level connectivity [Fletcher et al.(2024)]— can provide guidance for conserving non-habitat areas of higher permeability (e.g., corridors or stepping stones) but also for identifying areas of low permeability as targets for restoration action, especially where habitat restoration has the potential to enhance overall connectivity [Brodie et al.(2025)].

Existing connectivity models belong to two broad categories that reflect the two components of connectivity: those that emphasize habitat patch connectivity and those that emphasize matrix permeability [Rayfield et al.(2011)]. Most habitat patch models tend to be inspired by graph theory (e.g., Conefor [Saura and Torné(2009), Urban and Keitt(2001)]) and calculate connectivity values between a focal habitat patch (e.g., a forest fragment) and every other patch in the landscape. It is important to note that, for habitat patch models to be ecologically appropriate, they must also consider intra-patch connectivity (i.e., allow for self-colonization of a patch) to avoid counterintuitive results [Spanowicz and Jaeger(2019)]. In comparison, landscape models account for differentials in *permeability* or *resistance* across the matrix that can help or hinder the dispersal of animals [Fletcher Jr. et al.(2019)]. They are often based on electrical circuit theory (e.g., Circuitscape/Omniscape) and simulate an electric current traversing a resistance matrix [McRae et al.(2008), McRae et al.(2016), Hall et al.(2021), Landau et al.(2021), McRae and Kavanagh(2011)]. Such models are useful for highlighting dispersal routes throughout the landscape [Rayfield et al.(2011)]. Both forms of model have been instrumental in enhancing our understanding of species dispersal and landscape connectivity, and have often been used to guide conservation and restoration decisions [Dickson et al.(2019), Correa Ayram et al.(2016), Minor and Urban(2008)]. However, existing constraints limit these models from meeting the global needs of decision makers.

Current habitat connectivity models are often computationally limited when run on large spatial and taxonomic scales, which is an issue when trying to scale up mapping efforts to hundreds of species [Liczner et al.(2024)]. For example, in a study of connectivity in North America, researchers showed that computation time scaled with dispersal distance, limiting the mapping of connectivity for long-distance dispersers such as birds [Belote et al.(2022)]. Recent efforts to map connectivity at larger spatial scales, such as a global assessment of protected area connectivity [Ward et al.(2020)], have focused on *structural connectivity*, which only accounts for the spatial configuration of habitat patches [Tischendorf and Fahrig(2000)]. Such a simplified approach ignores inter-specific variability in how populations use and move across the landscape—i.e., *functional connectivity*—and understates the widely recognized importance of the landscape matrix [Watling et al.(2011), Fletcher et al.(2024), Bueno et al.(2026)]. A more recent global effort mapped functional connectivity for protected areas using tracking data for 48 mammal species [Brennan et al.(2022)] but, despite the recognized importance of multi-species connectivity models

[Wood et al.(2022)], the mapping of functional connectivity has been historically limited because existing models require detailed input data (e.g., tracking or gene flow) which only exist for a handful of species. In addition to computational challenges and data limitations, most habitat connectivity models are not tested for ecological realism. For example, only 2.5% of connectivity models used in scientific publications report any validation [Creech et al.(2024)]. Some models, particularly for mammals, are validated using tracking data [Phillips et al.(2021), Zeller et al.(2018)], but these data are not widely available across taxa, highlighting the need for widely applicable model validation with independent data.

To contribute to the task of mapping functional habitat connectivity at broad spatial and taxonomic scales in order to guide conservation and restoration priorities, we present EcoScape, an algorithm that computes habitat connectivity based on species-specific dispersal abilities and habitat preferences. EcoScape models the propagation of populations across landscapes, outputting both a connectivity raster and a flow raster: the former emphasizes intra- and inter-patch habitat connectivity, while the latter focuses predominantly on highlighting dispersal paths between habitat patches. From the connectivity raster, one can then estimate a species' Functionally Connected Habitat (FCH) i.e., the amount of its range that is connected. EcoScape can be parameterized for diverse taxa using widely available open-source datasets including functional traits and occurrence data, though we demonstrate its use with birds. The computation is performed via a novel dispersal algorithm that leverages the parallelism provided by modern Graphical Processing Units (GPU)s.

Here, we outline EcoScape's inputs, algorithm calculations, and outputs, as well as the python package for its public use. Demonstrating EcoScape's computational speed, we compute connectivity and flow over the contiguous United States for three example resident forest-dependent birds: Acorn Woodpecker (*Melanerpes formicivorus*), Pileated Woodpecker (*Dryocopus pileatus*), and Steller's Jay (*Cyanocitta stelleri*). We then provide validation support for EcoScape's habitat connectivity results using data from the community science platform eBird [Sullivan et al.(2009)]. Through this efficient algorithm and data workflow, we aim to provide scalable habitat connectivity analysis at both fine spatial resolutions and continental extents, and for a large suite of species, in order to guide conservation and restoration action.

2 Methods

We first describe the EcoScape algorithm including its inputs, computation, and outputs (Figure 1). We then test EcoScape on three focal bird species across the contiguous United States. Finally, we validate the EcoScape connectivity estimates for the focal species using occurrence data from eBird.

2.1 EcoScape Overview

EcoScape is a pixel-level habitat connectivity algorithm that simulates the propagation, or spread, of animal populations across landscapes (Figure 1). For a given focal species, EcoScape assumes that there is primary habitat (often configured into habitat patches), within which individuals can move freely (Figure 2A–C.), and a non-habitat matrix of varying degrees of permeability that differentially affects the spread of the population between habitat patches (Figure 2D–G.).

In a given simulation, populations are seeded randomly in habitat pixels; they then propagate throughout the landscape by spreading from pixel to neighboring pixels. How far they can spread is ultimately determined by a species' dispersal ability, but differences in permeability among land cover types may facilitate or inhibit propagation between patches of habitat. For example, a forest-dependent species might spread freely through forest and easily through a plantation, but be unable to spread through desert. After iterating over hundreds of simulations, EcoScape produces two outputs. First, *connectivity* values in essence show how well-connected habitat pixels are to each other, with pixels in smaller or more isolated habitat patches receiving lower connectivity values. Second, *flow* values indicate how important different parts of the matrix are in facilitating propagation between habitat patches. For example, for a forest species, pixels in a corridor of secondary vegetation may receive high flow values while pixels in a cattle pasture receive low flow values.

Conceptually, EcoScape shares similarities with widely used habitat connectivity algorithms based on graph theory [Urban and Keitt(2001)] and circuit theory [McRae and Beier(2007)], but estimates and computes connectivity and flow in distinct ways. Similar to graph-theory approaches, EcoScape considers habitat patches to be sources of populations which then disperse between patches. However, in graph theory, connectivity values are patch-level, only one pathway (usually the shortest path) of connection is considered, and the role of the matrix is either implied, or ignored [Moilanen(2011)]. In comparison, circuit-theory approaches consider multiple pathways of dispersal from a source habitat patch to every other patch in the landscape, with an explicit consideration of the permeability of the landscape matrix, modeling movement as electrical current in a landscape with given resistance [McRae and Beier(2007)]. However, circuit-theory models require solving circuit equations which limits the options for parallelization. EcoScape adopts a propagation-based approach that can be seen as a bridge between these two types of models: its connectivity output resembles those from graph-theory models, while the flow output retains a multi-path, permeability-driven perspective akin to circuit-theory models. In particular, EcoScape forfeits

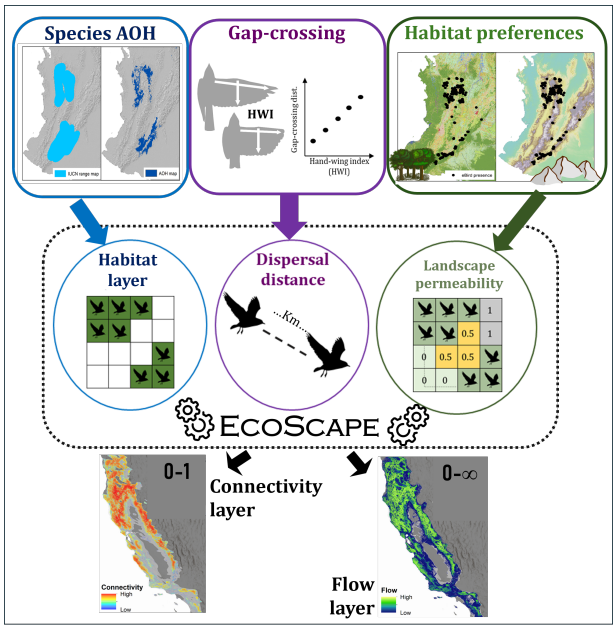

Figure 1. EcoScape flowchart showing the sources used to produce species-specific inputs (habitat layer, dispersal distance, and landscape permeability) and output layers (connectivity and flow).

circuit-based models in favor of a simulation approach which leverages the massive parallel processing capabilities of modern GPUs.

EcoScape is ecologically informed and species-specific in that it incorporates species' habitat preferences—which determine both what is considered "habitat" as well as permeability through other land cover types—and their dispersal ability. However, EcoScape does not directly model individual movement, decision making processes, or mortality, which differentiates it from Individual-Based Models (IBMs), such as those based on Markov chain theory [Fletcher et al.(2023)]. Instead, the focus is on mapping at a population level the possible and probable dispersal paths and resulting connectivity across a landscape. The inputs for the EcoScape algorithm can potentially come from a variety of user-defined sources, including detailed animal tracking or mark-recapture studies, but we present a version which relies only on widely available open-source data to showcase its applicability to a broad range of bird species.

2.1.1 Inputs and Outputs. The input to EcoScape includes two spatial raster layers: a *habitat* layer h and a *landscape permeability* layer p (Figure 1). The *habitat* layer is a fine-grain representation of a species' *area of habitat* (AOH), i.e., the suitable habitat within its distribution [Brooks et al.(2019)]. A habitat pixel h_{ij} at coordinates i, j can have value 0 (non-habitat) or 1 (habitat). The *permeability* layer is a representation of how likely a species is to successfully propagate through that land cover type according to its land cover preferences. The landscape permeability p_{ij} at a pixel ij has values in the interval $[0, 1]$: 0 indicates no possibility of species propagation, and 1 indicates full possibility of propagation. Thus, permeability is inversely related to the standard matrix resistance [McRae et al.(2008), McRae et al.(2016)]. We assume that the permeability of pixels in primary habitat is 1, such that $p_{ij} = 1$ when $h_{ij} = 1$.

The model also takes as input the total dispersal distance d of the species, which indicates how far the population can propagate from a seeded habitat location in the landscape. In a landscape of pure habitat, d represents the maximum distance (i.e., total number of pixels) over which the species can propagate, where propagation occurs over one pixel per propagation round (see below). For example, a species where $d = 10$ will propagate over ten rounds, with a maximum dispersal distance of 10 pixels from the initial seed. This dispersal distance can be either a fixed number of pixels, or a number of pixels drawn from a probability distribution, allowing for a more realistic range of dispersal distances. In particular, the half-Cauchy distribution, with its long tail, is a suitable distribution that enables the inclusion of more rare, long-distance dispersal events [Paradis et al.(2002)].

EcoScape outputs two raster layers. The first is a *connectivity* raster c, where $0 \leq c_{ij} \leq 1$ represents the probability that a habitat pixel ij can be repopulated. A habitat pixel with a higher connectivity value is more likely to be repopulated over the simulated propagation rounds. The second is a *flow* raster f, where f_{ij} represents the relative importance of each pixel in being a conduit for propagation between habitat pixels. A matrix pixel with a higher flow value indicates a pixel that contributed to more downstream propagation of habitat. In other words, the *connectivity* raster is important for showing how well-connected habitat patches are, and the *flow* raster is important for showing how well different parts of the matrix act to facilitate connectivity between habitat patches.

2.1.2 Computing Connectivity. To compute connectivity, EcoScape runs a series of simulations to model how a species can repopulate its habitat via dispersal from randomly chosen habitat seed locations. Rather than modeling individual animals, EcoScape evaluates the population's overall capacity to reach other habitat locations, averaging the results of all simulation runs. At the start of each simulation, we choose the maximum propagation distance n, measured in pixels, via $n = d$ if d is fixed, and via $n \sim d$ if d is a probability distribution of distances. Once n is chosen, we choose the seeds of the propagation by sampling habitat pixels randomly and independently with probability $1/n^2$, yielding an average of one seed for every n^2 habitat pixels, so that the inter-seed distance is comparable to the propagation distance. This seed density ensures that propagation originating from

different seeds seldom overlap, yielding a better modeling of species dispersal. We initialize a *repopulation* raster layer r, setting it to 1 at seed pixels and to 0 everywhere else.

Once the seeds are chosen, the simulation performs n rounds of propagation, during which the population can propagate from a pixel to any of its 8 neighbors. These repopulation propagation rounds are not meant to directly model animal movement: they model reachability from a seed location, taking into account dispersal ability, habitat preferences, and multi-path propagation.

To induce randomness in the paths taken by the propagation, the population at a pixel does not propagate to all 8 neighbors at once: rather, we use coin tosses to choose only *some* of its 8 neighbors to be reached in each round. This induces variability in the paths taken by the dispersal in each simulation, so that when the results from multiple simulations are averaged, the result reflects a proper multi-path modeling of the dispersal process [McRae et al.(2008), Panzacchi et al.(2016), McRae and Beier(2007)]. Since every pixel can typically be reached from a seed in multiple ways, the random coin tosses do not appreciably decrease the dispersal radius n, and indeed ensure a roughly circular dispersal pattern, despite the underlying grid topology of the pixels (see Supplementary Information S1.2).

Precisely, at each round of propagation we compute an updated repopulation raster r' via:

$$r'_{ij} = \max\left\{ r_{ij},\ X_{ij} \cdot p_{ij} \cdot \max_{kl \in N(ij)} \left(Y_{kl} \cdot r_{kl}\right) \right\}, \qquad (1)$$

and then we set $r := r'$, ready for the next round. In Eq. (1), $p_{ij} \in [0, 1]$ is the landscape permeability of pixel ij, $N(ij)$ is the 3×3 pixel patch with center ij, $X_{ij} \in \{0, 1\}$ is the outcome of the coin toss selected from $\{0, 1\}$ with equal probability, and Y_{kl} is a random variable chosen uniformly in $[1 - 10^{-4}, 1]$. In short, the new value of the pixel is taken as the maximum of either the pre-existing pixel value or any successful propagation into the pixel from neighboring pixels. For example, consider an unpopulated pixel ij with permeability $p_{ij} = 0.5$, adjacent to a pixel kl with repopulation $r_{kl} = 0.8$. If the coin toss at ij yields heads, so that $X_{ij} = 1$, and kl provides the maximum in (1), then ij is repopulated with $r'_{ij} = 0.5 \cdot 0.8 = 0.4$, up to the negligible tie-break factor Y_{kl}. Repopulation thus attenuates as it spreads across less permeable land cover. Crucially, (1) can be implemented using primitives that have been highly optimized for GPUs: namely, products and point-wise maxima of rasters, and max-pool operators (to compute $\max_{kl \in N(ij)}$) [Chetlur et al.(2014)].

The random variable Y_{kl} serves as an important tie-break for when multiple neighboring pixels of ij share the same value of repopulation r. When we increase the repopulation at a pixel ij, that is, when $r'_{ij} > r_{ij}$, we wish to attribute the source of propagation to one of the neighbors of ij, enabling us to compute propagation paths, and the repopulation *flow* described later. If multiple neighbors of ij have the same value of repopulation (e.g., 1), it is impossible to attribute a single origin of repopulation. The random variable Y acts as a tiny tie-break: by affecting each neighbor differently, it ensures that the $\max_{kl \in N(ij)}$ in Eq. 1 has only a single neighbor $kl \in N(ij)$. As an additional refinement, we apply the update Eq. 1 only if the value r_{ij} would increase by at least 0.05 as a result. This ensures that propagation paths are attributed due to functionally significant repopulation increases and are not then re-attributed due to marginal increases (e.g., from 0.8 to 0.800001). It also ensures that unpopulated pixels do not become repopulated by very small amounts.

Finally, the *connectivity* layer c is obtained by computing the average $\bar{r}$ of r over hundreds or thousands of simulations and by clipping the result to the habitat via $c = h\bar{r}$ (i.e., $c_{ij} = h_{ij}\bar{r}_{ij}$ at every pixel ij). Thus, $c_{ij} = 0$ if $h_{ij} = 0$, and $0 \le c_{ij} \le 1$ if $h_{ij} = 1$. In other words, we only consider connectivity *within* habitat. We have implemented the connectivity computation in Python, using the PyTorch machine-learning framework [Paszke et al.(2019)], which provides support for GPU processing.

2.1.3 Computing Functionally Connected Habitat.

While the connectivity layer produces pixel-level connectivity values across a landscape or species' range, it is useful to derive summary statistics representing overall connectivity. In particular, given the extent of suitable habitat within a region or across a species' range, it is useful to know how much of that habitat is functionally connected. We therefore define the *functionally connected habitat* (FCH) as $FCH = a \sum_{ij} c_{ij}$, where a is the area of a pixel. In this sum, every habitat pixel contributes an area amount proportional to the pixel's connectivity value. When considering different species within the same extent of habitat, FCH becomes a directly comparable measure of how well-connected that habitat is for each species. FCH is related to the widely used Equivalent Connected Area (ECA) from graph-theory models i.e., the amount of habitat that is reachable in the landscape, usually reported as an area value [Saura et al.(2011)] (see details in Supplementary Information S1.3). To control for the extent of habitat—where the total area of habitat is $H = a \sum_{ij} h_{ij}$—we define the *connected fraction* as $CF = FCH/H$ which expresses FCH as a percentage of the area of habitat that is functionally connected.

2.1.4 Computing Flow.

The flow layer indicates the relative importance of each pixel to habitat repopulation. Specifically, the flow f_{ij} through pixel ij represents the amount of downstream repopulation due to dispersal paths through pixel ij and it only considers dispersal events that ended in repopulation of another habitat patch. For instance, if a 10×10 area is repopulated to value 0.7, and all repopulation paths go via pixel ij, the flow through ij would be

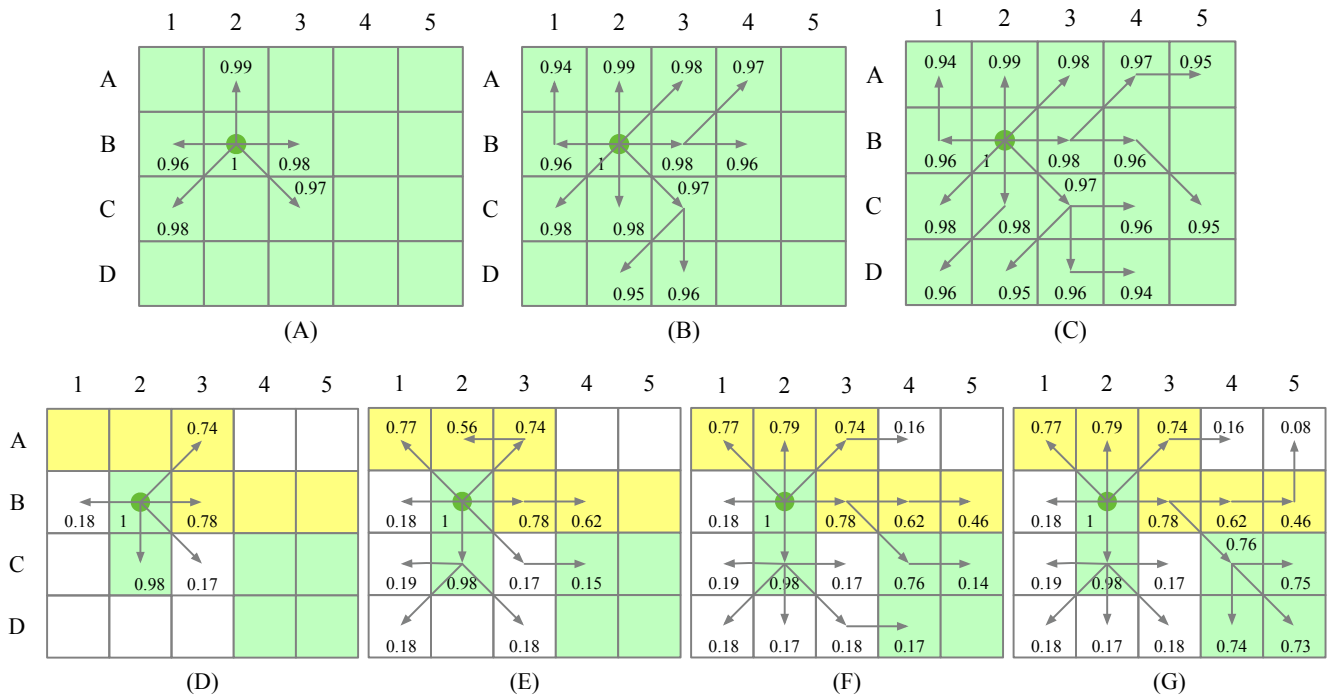

Figure 2. Examples of repopulation propagation from a seed in B2. Pixels are labeled with their repopulation value, and arrows indicate the direction of propagation. In (A), (B), (C), the propagation occurs entirely within a habitat with permeability 1. In (A), only 5 of the 8 neighbors of the seed are repopulated, corresponding to where the random coin toss X had outcome 1. Similarly, in (B) and (C), only some of the neighbors of repopulated pixels are themselves repopulated. The small random decreases in repopulation at each propagation are due to the tie-breaking random variables Y. In (D), (E), (F), (G), the propagation occurs across habitat (in green), a landscape corridor with high permeability 0.8 (yellow), and less favorable land cover with permeability 0.2 (white). In (F), note how the value at pixel A2 increased due to direct propagation from the seed at pixel B2, superseding the previous value attained from A3. Similarly, in (G) pixels D4 and C5 gain repopulation due to a more direct propagation path. These increases due to path revisions do not occur in (A), (B), (C), since all such revisions would lead to repopulation increases below the 0.05 threshold.

$0.7 \cdot 100 = 70$. Unlike connectivity, the *flow* can be nonzero outside of the habitat. The flow value at pixels outside the habitat thus yields information on the role of landscape matrix in maintaining connectivity, which has been widely recognized as ecologically important [Fletcher et al.(2024)]. In the Supplementary Information S1.1, we show how the flow can be efficiently computed via the gradient backpropagation mechanism of machine-learning frameworks such as PyTorch.

2.1.5 Computation for a Synthetic Landscape. We illustrate the EcoScape computation of connectivity and flow across a hypothetical landscape in 3. In this landscape there are six habitat patches that differ in size, with some being bridged by high permeability land cover. The pixel permeability is 1 in the habitat pixels (e.g., primary forest), 0.98 in the landscape corridors (e.g., agroforestry), and 0 elsewhere. The computation was performed on a 40×60-pixel region, using dispersal distance 100 and seed density 400; connectivity and flow were computed averaging 1000 simulations. Here, we used a higher-than-normal value of seed density to emphasize how connectivity outputs vary according to a patch's size and degree of isolation. We display the value of the flow layer on log-scale, as $\hat{f} = 20 \log_{10}(1 + f)$.

2.2 Applying EcoScape to Focal Species

We used EcoScape to compute the connectivity and flow layers throughout the contiguous United States (US) for three resident forest-dependent bird species: Acorn Woodpecker (*Melanerpes formicivorus*; ACWO), Pileated Woodpecker (*Dryocopus pileatus*; PIWO), and Steller's Jay (*Cyanocitta stelleri*; STJA). We chose these three focal species to represent a range of dispersal abilities (see below) and forest dependencies, and due to their broad but different distributions across the US. The fact that these are relatively large species (65–350 g) also means that they would be able to

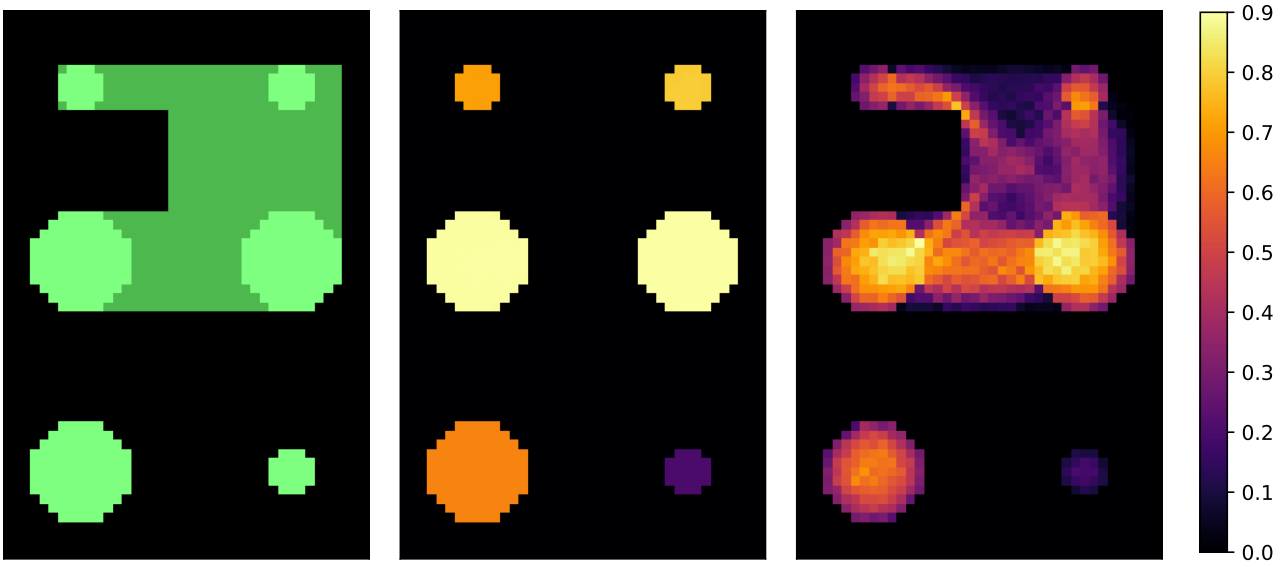

(A) Land cover layer **(B)** Connectivity layer **(C)** Flow layer

Figure 3. EcoScape connectivity computation on a synthetic 40×60-pixel habitat and landscape matrix. (A): Land cover input layer: habitat patches (in light green) are connected by high permeability corridors (in green), surrounded by low permeability matrix (in black). (B): Connectivity output layer: lighter colors indicate higher connectivity. Larger patches have higher connectivity; for equal-sized patches, patches connected by more permeable land cover have higher connectivity than isolated patches. (C): Flow output layer: in log scale, with lighter colors indicating higher flow. Multiple paths connect habitat patches according to the landscape matrix permeability. The color ramp pertains to panels (B) and (C).

carry GPS devices [Wikelski et al.(2007)], enabling future validation with tracking data.

2.2.1 Land Cover Inputs. We used the Jung et al. (2015) global habitat map [Jung et al.(2020)] to produce the habitat and land cover permeability layers for the three species across the US. This map classifies global land covers into the habitat types described by the IUCN Red List Habitats Classification Scheme [IUCN(2023)]. For this example, we used the level 2 habitats, e.g., "Forest: Temperate", "Shrubland: Mediterranean". To compute habitat and landscape permeability across the US for each of the three example species, we prepared input rasters independently for each US state, including a buffer of 100 km around each state. For each state, we re-projected and cropped the original raster to a conformal Mercator projection (EPSG:3857) scaled so that pixels in the state center correspond to 300 × 300 m on the Earth's surface. Using a Mercator projection preserves the local geometry and models isotropic species dispersal; the area effects are negligible, since the projection is scaled independently for each US state. The original raster from Jung et al. has a resolution of 100 m but we resampled it to 300 × 300 m, choosing this resolution to factor in the trade-offs of ecological realism and computational efficiency. Given that computation times increase with the number of propagation rounds, reaching a 3-km dispersal distance over 10 pixels of 300 m is much more computationally efficient than reaching it over 30 pixels of 100 m. For temperate forest birds, 100 m is also a relatively small distance, and we did not want to create impassable barriers that were that narrow, while 1 km may be too far to disperse for some species; thus, a common resolution of 300 m reflects this compromise.

2.2.2 Area of Habitat. To create the habitat layer, we started with the range maps for the species, which can be downloaded from the community-science platform eBird at https://science.ebird.org/en/status-and-trends/range-maps. As our species are forest-dependent, we refined these ranges by forest availability using the land cover map described above; for the Acorn Woodpecker, we further included the "Shrubland: Mediterranean" land cover type (IUCN code: 308) as suitable habitat, which corresponds to sparse oak woodland in the western US, a primary habitat for the species. This process resulted in a 300×300m boolean (0, 1) raster encoding the AOH for each species.

2.2.3 Occurrence Data. To parameterize permeability, we sourced species occurrence data from eBird [Sullivan et al.(2009)] . eBird data are organized into *checklists*, where every checklist records a date and location, species identity and count, as well as effort related to the

sampling method ("traveling", "stationary", "incidental"), duration, distance, number of observers, and whether the checklist is "complete" (i.e., whether the observer reported every species of bird seen or heard). For landscape permeability, we focused on complete checklists with traveling protocol submitted during 2012-2018 (to match the time frame of the land cover map) and only included checklists with distances $<\sim$ 2km (to match the spatial resolution of the raster data).

2.2.4 Landscape Permeability. To produce the landscape permeability raster for each species, we started from the species' habitat preferences given in the IUCN Red List. This dataset provides lists of "major importance" and "suitable" land cover types for each species. For example, forest could be a land cover of major importance, while shrubland could be a suitable land cover. We produced a preliminary assignment of permeability $\tilde{p}$ to each land cover class as follows. We assigned permeability $\tilde{p}_i = 1$ (no resistance) to land cover types i that correspond to forest or other habitats of major importance for the species; these land cover types are then the *habitat land cover types*. Next, we assigned permeability $\tilde{p}_i = 0.9$ to land cover types i that are listed as suitable for the species. Finally, all other land cover types i were assigned permeability $\tilde{p}_i = 0$.

We then refined this initial assignment for each species using information on the species' documented habitat use via occurrence data from eBird, as follows. Let B_F of a focal species be the average count per checklist reported in a given habitat land cover type (e.g., forest). For a non-habitat land cover type i (e.g., wetlands), let B_i be the average count of a particular species reported per checklist in that non-habitat land cover. If $B_i > B_F$, we set $\hat{p}_i = 1$. If $B_i \leq B_F$, we set $\hat{p}_i = \max(\tilde{p}_i, B_i/B_F)$. The resulting permeability $\hat{p}$ is per kilometer; the permeability per pixel is therefore obtained as $p_i = \hat{p}_i^{0.3}$, where 0.3 is the pixel size in kilometers. We report the details of the computation of B_F and B_i, and the permeability values used for all land cover classes in the study, in Supplementary Information S1.4.

2.2.5 Dispersal Distances. Values of dispersal distance are hard to encounter in the literature and exist only for a few well-studied birds [Fraser et al.(2018)]. However, recent proofs-of-concept have elucidated a relationship between dispersal distance and a species' hand-wing index (HWI) [Sheard et al.(2020), Arango et al.(2022)]. HWI is a measure of wing shape, where species with a higher HWI have longer, more pointed wings that confer a greater dispersal ability. Importantly, we wanted a measure of dispersal ability that could, in principle, be applied to any bird species in the world (including the vast majority that lack empirical observations of dispersal), and the recent release of the global AVONET database [Tobias et al.(2022)] provides HWI for all the world's birds. Next, we used empirical dispersal data for 114 bird species from [Weeks et al.(2022)], species which are found across a range of latitudes and systems. From these data we computed the best linear fit, with zero intercept, between dispersal distance d (in km) and HWI; the resulting linear relation was $d = 0.49 \cdot HWI$. From this, given a pixel size of 300 m, we set the dispersal distance to $d = 45$ (13.5 km), 22 (6.6 km), 42 (12.6 km) pixels for the Acorn Woodpecker, Pileated Woodpecker, and Steller's Jay, respectively.

We computed connectivity using both dispersal distances fixed to the above values, and dispersal distances sampled from a half-Cauchy distribution with a mean of d, which we then truncated to a maximum of $4d$ pixels. The use of the half-Cauchy distribution allows for a more realistic modeling of the dispersal distance as it permits the possibility of long-distance dispersal events [Paradis et al.(2002)]; however, the truncation is necessary to bound the amount of required GPU memory.

2.2.6 Computation Settings. EcoScape processes the input habitat and landscape matrix permeability rasters state by state, using the state-centered Mercator projection and the 300×300 m grid mentioned above for each state. Each state raster is processed by subdividing it into fixed-sized *tiles* of $n \times n$ pixels and by processing each tile independently; the resulting output tiles are then combined. The size of the tiles is chosen to ensure the simulations for each tile fit in the GPU memory. For each $n \times n$ tile, EcoScape is fed habitat and permeability inputs of size $(n + 2b) \times (n + 2b)$ pixels, consisting of the $n \times n$ tile interior and of a border of width b all surrounding the tiles. The border is used to provide context for the computation and must be at least as large as the largest dispersal distance considered in the simulations. Specifically, when d is a pixel amount, we use $b \geq d$. When d is a half-Cauchy distribution, we take b to be greater than its truncation value. For each tile, EcoScape performs 1000 simulations and averages the results, producing an $n \times n$ output; the outputs are then combined to form the output rasters. The simulations are performed in parallel batches to optimize GPU usage.

We computed the connectivity and flow layers running EcoScape on an NVidia A100 GPU with 40 GB of memory, on Google Colab Pro. The values of the parameters n and b, and the batch sizes we used, are reported in Supp. Table S2. EcoScape can be used to compute connectivity only, or both connectivity and flow. When computing only connectivity, the GPU memory requirements depend only on the input size $(n + 2b)^2$; when also computing the flow, the GPU memory requirements are proportional both to the input size and to the dispersal distance d, requiring the use of smaller tiles.

2.3 Validating EcoScape with Occurrence Data

In order to evaluate the efficacy of EcoScape, we sought to model whether EcoScape-derived connectivity estimates could predict local abundances of our three focal species across forested grid cells in the contiguous

United States. We hypothesized that better-connected habitat should support a more abundant population, resulting in higher checklist counts for a species in a given landscape [Martensen et al.(2012)]. For abundance data we again used checklists from eBird (see Supplementary Information S2.1 for details). However, there is an important distinction between how we use eBird for validation vs permeability. For permeability, *occurrence* was modeled *between land cover types*, and was assumed to be 1 for forest. In contrast, for validation, we are interested in whether EcoScape can predict differences in *abundance within habitat*, and thus within forest. In addition, permeability was based on year-round occurrence use while validation considered only abundance during the breeding season i.e., between dispersal events.

After filtering and processing the eBird data (Supplementary Information S2.1), we used an AIC-based multi-model inference approach [Anderson and Burnham(2004)] to assess whether connectivity estimates could predict checklist counts in grid cells (for more details, see Supplementary Information S2.2). Briefly, we built a series of competing models with different combinations of covariates and evaluated their support based on ΔAIC values and model weights. All models included counts as the response variable in a generalized linear model (GLM), with a negative-binomial error structure (log-link) to account for overdispersion. We built five models: a *null model* with no predictors; an *effort-only model* containing predictors of eBird effort; an *area model* containing effort plus forest patch area; a *connectivity model* containing effort plus our EcoScape connectivity values; and a *full model* containing both area and relative connectivity given area.

2.4 Sensitivity Analyses

To further interrogate the ability of EcoScape to model habitat connectivity across forested landscapes, we carried out a series of sensitivity analyses. In the first sensitivity analysis we tested whether varying the number of simulations affected our results. We found that using 100 simulations (instead of the default 1000) resulted in very similar connectivity estimates (Supplementary Information S3.1)

In the second set of sensitivity analyses we varied the permutations that went into the EcoScape algorithm itself. First, we ran a version of EcoScape where n was fixed as d (i.e., not drawing from a half-Cauchy; (Supplementary Information S3.2)). We also quantified and compared computation times for this version. Second, to assess whether the scaling of dispersal distances mattered, we ran two versions where $n = 2d$ and $n = 0.5d$ (Supplementary Information S3.3). Third, to test the importance of including the permeability layer, we ran EcoScape with default parameters but where permeability was fixed at 0 outside habitat (Supplementary Information S3.4). For all three analyses we ran validation models with identical structures to the the default connectivity models and compared them via AIC.

In the third set of sensitivity analyses, we considered two alternate response variables in our validation models and whether the model rankings would change accordingly (Supplementary Information S3.5). First, we considered *average abundance* i.e., the average number of individuals on checklists in each grid cell. Second, we considered *occurrence probability* i.e., the proportion of checklists in each cell that recorded at least 1 individual.

Finally, we chose to compare our EcoScape-derived connectivity estimates with estimates of *cumulative current* computed from Omniscape [Hall et al.(2021)], a leading habitat connectivity algorithm (Supplementary Information S4). We compared the state-by-state computation times for our three species between EcoScape and Omniscape (Supplementary Information S4.1). We also included the estimates of cumulative current in validation models which we then compared within our main model set (Supplementary Information S4.2).

3 Results

3.1 Connectivity and Flow for the Simulated Landscape

Running EcoScape on a synthetic landscape exemplifies the role of patch size, distance between patches, and permeability of the matrix in determining the connectivity of habitat patches and the flow between them (Figure 3). In the synthetic landscape, connectivity values exist only within habitat and vary for patches of different sizes and distances from other habitat patches (Figure 3B). For example, a large, isolated patch (bottom left) could repopulate itself, while a small, isolated patch (bottom right) was less able to. Large patches that are separated by a permeable matrix (darker green) had higher connectivity (central row) than those isolated by impermeable matrix (black). Small patches separated by permeable matrix (darker green) had higher connectivity even than a large isolated patch because they could be repopulated by neighboring habitat patches (top row).

Flow between patches was non-existent when the matrix was impermeable (black), and high when the matrix was permeable (darker green) (Figure 3C). Flow was higher between larger patches (central row) than between smaller ones, and was also higher for more direct paths between patches than for surrounding matrix. This proof-of-concept shows that EcoScape predicts population spread as one would expect given the principles of movement and landscape ecology [Prugh et al.(2008), Brodie and Newmark(2019)].

3.2 Connectivity and Flow for Focal Species

We demonstrate the use of EcoScape for three forest-dependent birds across the contiguous US. For Acorn Woodpecker (Figure 4A), Pileated Woodpecker (Figure 4C), and Steller's Jay (Figure 4B), the connectivity outputs showed clear spatial variation in habitat connectivity throughout each species' ranges. Habitat patches that are small and

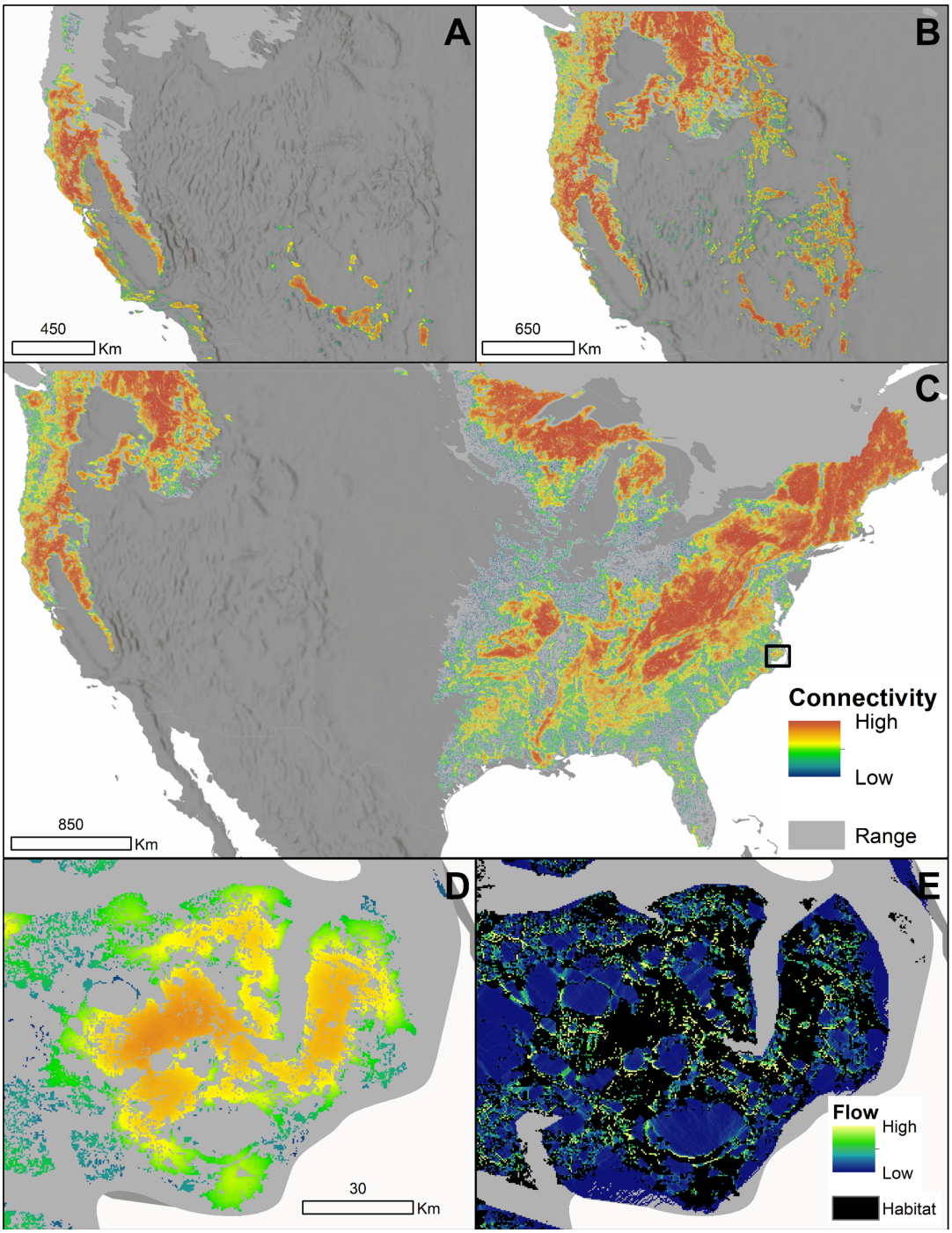

Figure 4. EcoScape outputs for three focal bird species across the contiguous United States. Connectivity is shown across the ranges of (A) Acorn Woodpecker, (B) Steller's Jay, and (C) Pileated Woodpecker. Insets show local connectivity (D) and flow (E) for Pileated Woodpecker for the black square in panel C.

isolated—including the Transverse Range in Southern California or the fragmented forests of the Southeast—showed lower connectivity than large, continuous forests—e.g., in New England and the northern Rocky Mountains. The two woodpecker species showed large swaths of highly connected habitat and their higher dispersal distance resulted in partially isolated fragments having higher connectivity than was the case for the lower dispersal Steller's Jay.

Detailed views of habitat connectivity and flow layers for the Pileated Woodpecker in North Carolina show the effects of patch size and isolation (Figure 4D–E). Large, contiguous patches had high connectivity values, whereas small and isolated ones showed low connectivity (Figure 4D). High values of flow indicate likely dispersal corridors between habitat patches (Figure 4E).

The computation of these continental-scale layers was very efficient. For Acorn Woodpecker, whose distribution spans five US states, adding up the computation times resulted in 68.7 seconds total. The distribution of Steller's Jay spans eleven states and the total run time was 21.14 seconds. The largest distribution was for the Pileated Woodpecker, spanning 35 states, resulting in a total run time of 417 seconds (~7 minutes). When compared to an alternative connectivity algorithm, Omniscape, EcoScape was on average 32x faster for these three focal species but produced similar spatially-explicit outputs (Supplementary Information S4.1 , Fig. S5).

3.3 Validation with Occurrence Data

For Acorn Woodpecker (n = 1623 grid cells), the model with the most support was the connectivity model, with a weight of 0.72 (Table 1A). In addition to the positive effects of number of checklists (0.81 ± 0.04 SE, Z = 17.97, $p < 0.001$), and average checklist duration (0.34 ± 0.05, Z = 6.60, $p < 0.001$), average connectivity positively predicted checklist counts (0.20 ± 0.04, Z = 4.47, $p < 0.001$). This result indicates that the local abundance of Acorn Woodpecker was on average higher in more well-connected forest (Figure 5A). With a ΔAIC of 1.98 and model weight of 0.27, the next best model was the full model where both patch area (0.15 ± 0.04, Z = 3.42, $p < 0.001$) and relative connectivity (0.13 ± 0.04, Z = 2.94, p = 0.003) positively predicted checklist counts, indicating that local abundance was higher within larger patches, and more so when those patches were more well-connected. The next best model after that was the area model with a ΔAIC of 9.13 and weight of 0.008.

For Pileated Woodpecker (n = 9626), the model with the most support was also the connectivity model , with a weight of 0.65 (Table 1B). In addition to the positive effects of number of checklists (0.69 ± 0.01, Z = 53.01, $p < 0.001$), average checklist distance (0.05 ± 0.02, Z = 3.51, $p < 0.001$), and average checklist duration (0.40 ± 0.02, Z = 25.83, $p < 0.001$), average connectivity positively predicted checklist counts (Figure 5B; 0.28 ± 0.01, Z = 20.93, $p < 0.001$). With a ΔAIC of 1.22 and model weight of 0.37, the next best model was the full model where both patch area (0.19 ± 0.01, Z = 13.58, $p < 0.001$) and relative connectivity (0.21 ± 0.01, Z = 15.73, $p < 0.001$) positively predicted checklist counts. The next best model after that was the area model with a ΔAIC of 228.94 and weight of <0.0001.

For Steller's Jay (n = 2308), the model with the most support was the full model, with a weight of 0.75 (Table 1C). Both the number of checklists (0.79 ± 0.03, Z = 25.49, $p < 0.001$) and average checklist duration (0.29 ± 0.04, Z = 8.30, $p < 0.001$) positively predicted checklist counts. Importantly, both patch area (0.24 ± 0.03, Z = 7.74, $p < 0.001$) and relative connectivity (0.19 ± 0.03, Z = 6.04, $p < 0.001$) also positively predicted local abundance, indicating that counts were higher within larger patches, especially when those patches were more connected. No other models occurred within 2 ΔAIC, although the connectivity model had a ΔAIC of 2.20 and a weight of 0.25 (Figure 5C).

For the sensitivity analyses, we found that varying the scaling of d made only small differences to connectivity values and their ability to predict local abundance (Supplementary Information S3.2, S3.3). However, as expected, entirely removing matrix permeability lowered model performance (Supplementary Information S3.4). The two alternate response variables (average count and occurrence probability) produced identical model rankings with qualitatively similar results (Supplementary Information S3.5). We can therefore be confident that our approach was not sensitive to the choice of response variable. Finally, we found that computing connectivity with EcoScape was much faster than computing cumulative current with Omniscape, and resulted in highly correlated estimates that better predicted local abundance for the three species (Supplementary Information S4).

From this multi-model process we can state that, for all three focal species, including EcoScape-derived connectivity estimates in models improved our ability to predict local abundances and occurrence probability beyond area effects alone.

4 Discussion

In an increasingly fragmented world [Zou et al.(2025)], there is a pressing need for scalable habitat connectivity modeling to inform conservation priorities [Beger et al.(2022), Zurell et al.(2025), Brodie et al.(2025)]. EcoScape is a species-specific ecologically informed, pixel-level algorithm to map functional habitat connectivity and flow at fine resolutions and continental scales using a population propagation framework. EcoScape generates outputs that provide insight into a species' use of both their primary habitat and the intervening landscape matrix. Specifically, it provides two complementary outputs: a connectivity layer which represents how well-connected different patches of habitat are,and a flow layer which highlights the most likely propagation paths between habitat patches (e.g., corridors and stepping stones). EcoScape considers species' habitat preferences and dispersal ability—which can be derived from open-source data platforms (e.g., IUCN, eBird, AVONET)—and thus produces a more ecologically informed representation of reality than is produced by simple structural connectivity models. While we have demonstrated its use for three wide-ranging forest bird species across the contiguous US, we emphasize that

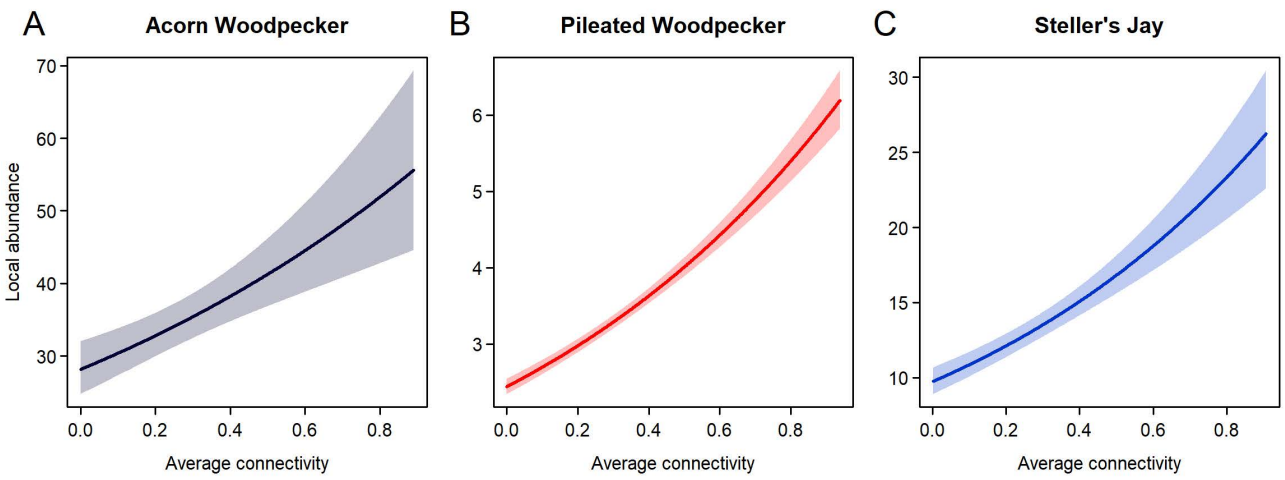

Figure 5. Local abundance of three focal bird species as predicted by habitat connectivity. Local abundance for (A) Acorn Woodpecker, (B) Pileated Woodpecker, and (C) Steller's Jay was summed across eBird checklists in every grid cell and modeled in a negative-binomial GLM as a function of eBird effort and habitat connectivity.

EcoScape can be applied to myriad other bird species, and potentially other taxa.

EcoScape's connectivity layer highlights the connectivity within habitat patches, resembling the patch-level connectivity metrics resulting from graph-theory connectivity models [Urban and Keitt(2001)]. Its flow layer explicitly considers the role of the landscape matrix, resembling the electrical current values resulting from circuit-based connectivity models [McRae and Beier(2007)]. Importantly, EcoScape can serve as a bridge between these two families of models because it produces both types of output in one single run [Fletcher et al.(2024), Bueno et al.(2026)]. However, EcoScape computes connectivity in distinct ways from graph- or circuit-theory models, and the processes it models are at the population level. EcoScape differs from IBMs [Bocedi et al.(2014)], spatially absorbing Markov chains (SAMCs) [Fletcher et al.(2023)], and other similar mechanistic models in that the latter explicitly predict individual movements considering behavior and decision making processes at different stages of dispersal, whereas EcoScape models the propagation or spread of populations over a landscape with differing degrees of permeability. In this way, EcoScape is more similar to diffusion models such as those used to model forest recovery [Acevedo et al.(2012)], but with the addition of considering the impact of the matrix and species' dispersal abilities. In short, the outputs of EcoScape can be interpreted as the multiple possible paths a population could take in order to disperse between habitat patches, or as a scalable approximation of the mechanistic dispersal processes of IBMs.

One of the major innovations of EcoScape is its computational approach which results in relatively high speed for the modeling of habitat connectivity and flow for large spatial extents. We show that it can be used to generate connectivity maps across the contiguous US in just under seven minutes for a wide-ranging species such as Pileated Woodpecker, significantly faster than other algorithms such as Omniscape [Landau et al.(2021)] (Supplementary Information S4.1). The efficiency of EcoScape stems in part from its use of GPUs to simulate the process of population propagation within and between habitat patches. In particular, because we split the landscape into tiles, each simulation for each tile can be fed into a GPU core, allowing for multiple tiles to be processed in tandem, after which we mosaic the tiles to produce a landscape-level output. These simulations are more efficient, and far easier to parallelize, than solving circuit equations, which is typically needed for models that consider source and sink patches [Urban and Keitt(2001)]. The efficiency of EcoScape brings within reach the ability to map connectivity and flow across continents for hundreds, if not thousands, of species in a relatively short amount of time [Farley et al.(2018), Brodie et al.(2025)].

Besides computational efficiency, our approach extends the ability to map functional habitat connectivity for diverse animals and to validate connectivity estimates using open-source data. In particular, birds—which are less often featured in connectivity studies (but see [Brodie and Newmark(2019)])—benefit from readily available data that span the avian tree. Semi-structured occurrence data are available for almost all bird species via eBird [Sullivan et al.(2009)] and these data can be used for both informing habitat preferences and validating connectivity estimates. Moreover, global trait datasets such as AVONET [Tobias et al.(2022)] and BIRDBASE

(A) Acorn Woodpecker

Model	No. checklists	Avg. distance	Avg. duration	Patch size	Avg. connect.	Rel. connect.	df	ΔAIC	Model weight
Connectivity	0.81	0.04	0.34	–	0.20	–	6	0	0.72
Full	0.81	0.04	0.34	0.15	–	0.13	7	1.98	0.27
Area	0.80	0.04	0.34	0.15	–	–	6	9.13	0.01
Effort-only	0.78	0.02	0.35	–	–	–	5	17.03	0.00
Null	–	–	–	–	–	–	2	467.96	0.00

(B) Pileated Woodpecker

Model	No. checklists	Avg. distance	Avg. duration	Patch size	Avg. connect.	Rel. connect.	df	ΔAIC	Model weight
Connectivity	0.69	0.05	0.40	–	0.28	–	6	0	0.65
Full	0.69	0.05	0.40	0.19	–	0.21	7	1.22	0.35
Area	0.68	0.05	0.42	0.20	–	–	6	228.94	0.00
Effort-only	0.67	0.02	0.43	–	–	–	5	418.26	0.00
Null	–	–	–	–	–	–	2	4096.31	0.00

(C) Steller's Jay

Model	No. checklists	Avg. distance	Avg. duration	Patch size	Avg. connect.	Rel. connect.	df	ΔAIC	Model weight
Full	0.79	0.05	0.29	0.24	–	0.19	7	0	0.75
Connectivity	0.78	0.05	0.29	–	0.29	–	6	2.20	0.25
Area	0.78	0.04	0.31	0.24	–	–	6	32.33	0.00
Effort-only	0.75	0.03	0.31	–	–	–	5	82.28	0.00
Null	–	–	–	–	–	–	2	847.38	0.00

Table 1. AIC-based multi-model comparison of the predictors of local abundance in three focal bird species. Local abundance was modeled in a negative-binomial GLM as a function of combinations of covariates including eBird effort, habitat patch size, and habitat connectivity. Local abundance was summed across eBird checklists in a grid cell. No. checklists is the number of checklists in that cell; Avg. distance is the average checklist distance; Avg. duration is the average checklist duration; Patch size is the size of the habitat patch to which that cell belongs; Avg. connect. is the average habitat connectivity across the cell; Rel. connect. is the relative habitat connectivity after controlling for patch size; df is the model degrees of freedom; ΔAIC is the difference in AIC between each model and the top-ranked model.

[Şekercioğlu et al.(2025)] can provide functional traits that ecologically inform EcoScape. Yet, although we initially devised EcoScape to run on bird species using globally available data, the algorithm can be easily adapted to other taxa or input data. For example, detailed tracking data—which are often available for mammals—could be used to parameterize both dispersal distances and habitat preferences (e.g., using resource selection functions [Richard and Armstrong(2010)]; see case study on African wild dogs [Hofmann et al.(2023)]). Similarly, while EcoScape could be parameterized based on one source of data (e.g., GPS data), it could then be validated with other data sources (e.g., genetic data [Daniel et al.(2023)]). Indeed, part of the reason for choosing our three focal species was to encourage future tracking studies of these suitably large birds in order to provide movement data to validate their connectivity and flow maps. Furthermore, future versions of the algorithm could parse out different components of dispersal and habitat suitability based on life-history stage [Bowler and Benton(2009)] or gap-crossing ability [Claramunt et al.(2022)], expanding its applicability to many other animal taxa, from large carnivores to butterflies, so long as the user has information on habitat preferences and dispersal ability.

In addition to a demonstration of EcoScape's use, we provide a validation of its habitat connectivity outputs using data from eBird [Sullivan et al.(2009)]. We show that connectivity estimates (which were informed by eBird data outside of primary habitat) can help predict occurrence and abundance of our focal species *within* habitat above and beyond what area effects alone would predict (though area effects are also strong predictors of abundance; Figure 5). Furthermore, our sensitivity analyses demonstrate the importance of including the land cover permeability layer, as well as the robustness of the algorithm to scaling dispersal distance

values (Supplementary Information). These results underscore the importance of a species' dispersal capacity for its persistence in fragmented landscapes [Ausprey et al.(2023)], as well as the key role that the landscape matrix plays in mediating the movement of species across the landscape [Fletcher et al.(2024), Bueno et al.(2026)].

Most connectivity models that have some sort of validation have been tested via simulation experiments [Unnithan Kumar and Cushman(2022)], using animal tracking data [Pullinger and Johnson(2010), Zeller et al.(2018)], and, more rarely, with genetic data [Mateo-Sánchez et al.(2015)]. In the case of tracking data, which is used for validation in 43% of connectivity studies [Creech et al.(2024)], there is typically limited data availability for the vast majority of species, and those data that currently exist, are mostly for large and charismatic fauna such as large carnivores and ungulates [Wikelski et al.(2007), McClure et al.(2016)]. This data limitation explains the fact that most prior validations (80%) have been performed on mammals, highlighting the obstacle of validating connectivity models for smaller and lesser known species. We demonstrate a validation approach using community science data that can potentially be applied to hundreds of species. However, we recognize the limitation that abundance is an imperfect proxy for demonstrating connectivity, and that many other factors affect local abundance [Martin(2001)]. We hope that EcoScape will be validated with movement or genetic data from birds as those become increasingly available.

Despite the demonstrated validation of EcoScape for our focal species, some limitations might restrict the ecological realism of its outputs. First, relying on the HWI-to-dispersal-distance relationship—which was based on 114 species from mostly temperate regions [Weeks et al.(2022)]—could be limiting. This functional relationship might vary taxonomically or biogeographically, and it might even vary within a species' range. In particular, the HWI measurements that we use to parameterize EcoScape are mean values from the AVONET database [Tobias et al.(2022)]. As such, these values could mask important intra-specific variation in dispersal ability, including variation among different subspecies and populations [Fan et al.(2024)] as well as critical differences between male and female dispersal [Mishra et al.(2018)]. Similarly, EcoScape does not consider individual behavior, which is typically the domain of mechanistic IBMs and process-based models [Bocedi et al.(2014), Hofmann et al.(2023)] so it is unable to predict individual movement through the landscape. Distinct stages of dispersal, demography, and mortality, which are often included SAMCs [Fletcher et al.(2023)] and other models, are therefore not considered in EcoScape, limiting its ecological realism. However, With more intra-specific data, users could parameterize and run EcoScape on different subpopulations or demographic groups such as males versus females or adults versus juveniles.

The use of community science data also presents challenges and biases due to the unstructured ways in which data are collected, resulting in differing degrees of quality and availability [Callaghan et al.(2019), Dickinson et al.(2010)]. One salient issue is that observers might report birds they detected in a certain land cover from a completely different one (e.g., a bird observed in the forest is reported from a grassy patch), and this could affect our estimates for landscape permeability. Another issue is the spatial distribution of eBird data, with some areas being over-sampled and others under-sampled [La Sorte and Somveille(2020), Backstrom et al.(2025), La Sorte et al.(2024)]. In an effort to mitigate these biases, we followed eBird best practices in filtering down checklists to semi-standardized effort [Johnston et al.(2021)], we controlled for the number of checklists when parameterizing permeability, and we accounted for variation in effort during the validation process. However, data limitations from eBird might affect which species can be modeled due to EcoScape's reliance on suitable sample sizes for permeability estimation. When these challenges arise, phylogenetic imputation might help to fill taxonomic gaps in data availability [Molina-Venegas(2024), James et al.(2021)].

Lastly, some equity and access issues might limit the full reach of EcoScape to our intended diversity of users [Tabor et al.(2025)]. To best take advantage of EcoScape's optimized model, users are advised to run it on GPUs. Although GPUs are now regularly found on most laptops, we caution that the speed of the algorithm depends largely on the quality of the GPU being used, which might vary according to the user's available device. However, we emphasize that the model can be run on devices with moderate power, it will just take longer to produce the outputs.

Efficiently mapping functional habitat connectivity for a variety of taxa could have far-reaching impacts for ecology and conservation [Brodie et al.(2025)], and EcoScape can be used to answer a plethora of ecological questions on how landscape elements and structure modulate species movement and dispersal. For example, is habitat connectivity higher in land-sharing landscapes vs land-sparing landscapes [Grass et al.(2019)]? Do stepping stones work just as well as corridors in facilitating connectivity [Gillies and St. Clair(2010)]? And does island biogeography theory lead to accurate predictions of patch occupancy in fragmented landscapes [Simberloff and Abele(1982), Brodie and Newmark(2019), Prugh et al.(2008)]? EcoScape also enables the explicit use of habitat connectivity to guide conservation decisions globally. Conserving, enhancing, and increasing habitat connectivity have been identified as important mechanisms in combating habitat loss, fragmentation, and climate change impacts [McGuire et al.(2016), Brodie et al.(2025)]. Increasing connectivity is also a priority to stop the erosion of genetic diversity, which has been documented for two thirds of the

species included in a recent meta-analysis of changes in genetic diversity over time [Shaw et al.(2025)]. To achieve global targets of increased connectivity at landscape scales, we must produce spatially explicit models that highlight areas of high value for conserving and restoring connectivity for multiple species [Koen et al.(2014), DeMatteo et al.(2023), Brodie et al.(2025)]. For example, EcoScape could be used to identify priorities for protected area establishment based on more well-connected habitat [Olds et al.(2012), Pither et al.(2023)]. It could also be used to simulate connectivity outcomes under different land-management strategies such as restoring habitat corridors or stepping stones [Montes-Rojas et al.(2024)]. Finally, in a world of climate-driven species re-distribution [Jennings et al.(2020)], EcoScape could be used to map and predict landscape level range shifts [Fredston et al.(2025), Chen et al.(2011)].

As the fields of ecology and conservation continue to expand into the world of big data [Farley et al.(2018)], technological challenges arise from processing and taking full advantage of the fine-resolution and large quantity of data available. EcoScape helps meet this challenge by providing users with an open, efficient, and ecologically informed way to map habitat connectivity and flow at various spatial scales for animal populations around the world. These advances will allow ecologists and conservation planners to fully consider a spectrum of lesser-known species and diverse land-use scenarios to answer pressing ecological questions and guide conservation and restoration action.

Acknowledgments: We thank Drs Blessing Kavhu and Whitney Hansen for helpful edits to the manuscript, and members of the Conservation Ecology Lab (Mushtaaq Ali, Julián Llano, and Ezra Garfield) for helpful discussions about the algorithm.

Data and Code Availability: The python package to run EcoScape can be installed via `pip install ecoscape-connectivity` from https://pypi.org/project/ecoscape-connectivity/. The code and data needed to reproduce the results are available at Zenodo at 10.5281/zenodo.15042583.

Funding statement: The development of the EcoScape algorithm was facilitated by a Google Research Grant.

References

[Acevedo et al.(2012)] Miguel A. Acevedo, Mariano Marcano, and Robert J. Fletcher. 2012. A Diffusive Logistic Growth Model to Describe Forest Recovery. *Ecological Modelling* 244 (Oct. 2012), 13–19. doi:10.1016/j.ecolmodel.2012.07.012

[Anderson and Burnham(2004)] David Anderson and Kenneth Burnham. 2004. Model Selection and Multi-Model Inference. *Second. NY: Springer-Verlag* 63, 2020 (2004), 10.

[Arango et al.(2022)] Axel Arango, Jesús Pinto-Ledezma, Octavio Rojas-Soto, Andrea M. Lindsay, Chase D. Mendenhall, and Fabricio Villalobos. 2022. Hand-Wing Index as a Surrogate for Dispersal Ability: The Case of the Emberizoidea (Aves: Passeriformes) Radiation. *Biological Journal of the Linnean Society* 137, 1 (2022), 137–144.

[Ausprey et al.(2023)] Ian J. Ausprey, Felicity L. Newell, and Scott K. Robinson. 2023. Dispersal Limitation Predicts the Spatial and Temporal Filtering of Tropical Bird Communities in Isolated Forest Fragments. *Functional Ecology* 38, 1 (2023), 179–193. doi:10.1111/1365-2435.14462

[Backstrom et al.(2025)] Louis J. Backstrom, Corey T. Callaghan, Hannah Worthington, Richard A. Fuller, and Alison Johnston. 2025. Estimating Sampling Biases in Citizen Science Datasets. *Ibis* 167, 1 (2025), 73–87. doi:10.1111/ibi.13343

[Beger et al.(2022)] Maria Beger, Anna Metaxas, Arieanna C. Balbar, Jennifer A. McGowan, Remi Daigle, Caitlin D. Kuempel, Eric A. Treml, and Hugh P. Possingham. 2022. Demystifying Ecological Connectivity for Actionable Spatial Conservation Planning. *Trends in Ecology & Evolution* 37, 12 (Dec. 2022), 1079–1091. doi:10.1016/j.tree.2022.09.002

[Belote et al.(2022)] R. Travis Belote, Kevin Barnett, Katherine Zeller, Angela Brennan, and Josh Gage. 2022. Examining Local and Regional Ecological Connectivity throughout North America. *Landscape Ecology* 37, 12 (Dec. 2022), 2977–2990. doi:10.1007/s10980-022-01530-9

[Betts et al.(2017)] Matthew G. Betts, Christopher Wolf, William J. Ripple, Ben Phalan, Kimberley A. Millers, Adam Duarte, Stuart H. M. Butchart, and Taal Levi. 2017. Global Forest Loss Disproportionately Erodes Biodiversity in Intact Landscapes. *Nature* 547, 7664 (July 2017), 441–444. doi:10.1038/nature23285

[Bocedi et al.(2014)] Greta Bocedi, Damaris Zurell, Björn Reineking, and Justin M. J. Travis. 2014. Mechanistic Modelling of Animal Dispersal Offers New Insights into Range Expansion Dynamics across Fragmented Landscapes. *Ecography* 37, 12 (Dec. 2014), 1240–1253. doi:10.1111/ecog.01041

[Bowler and Benton(2009)] Diana E. Bowler and Tim G. Benton. 2009. Variation in Dispersal Mortality and Dispersal Propensity among Individuals: The Effects of Age, Sex and Resource Availability. *Journal of Animal Ecology* 78, 6 (Nov. 2009), 1234–1241. doi:10.1111/j.1365-2656.2009.01580.x

[Brennan et al.(2022)] A. Brennan, R. Naidoo, L. Greenstreet, Z. Mehrabi, N. Ramankutty, and C. Kremen. 2022. Functional Connectivity of the World's Protected Areas. *Science* 376, 6597 (2022), 1101–1104.

[Brodie et al.(2025)] Jedediah F. Brodie, Andrew Gonzalez, Jayasilan Mohd-Azlan, Cara R. Nelson, Gary Tabor, Divya Vasudev, Katherine A. Zeller, and Robert J. Fletcher. 2025. A Well-Connected Earth: The Science and Conservation of Organismal Movement. *Science* 388, 6745 (April 2025), eadn2225. doi:10.1126/science.adn2225

[Brodie and Newmark(2019)] Jedediah F. Brodie and William D. Newmark. 2019. Heterogeneous Matrix Habitat Drives Species Occurrences in Complex, Fragmented Landscapes. *The American Naturalist* 193, 5 (May 2019), 748–754. doi:10.1086/702589

[Brooks et al.(2019)] Thomas M. Brooks, Stuart L. Pimm, H. Resit Akçakaya, Graeme M. Buchanan, Stuart HM Butchart, Wendy Foden, Craig Hilton-Taylor, Michael Hoffmann, Clinton N. Jenkins, and Lucas Joppa. 2019. Measuring Terrestrial Area of Habitat (AOH) and Its Utility for the IUCN Red List. *Trends in ecology & evolution* 34, 11 (2019), 977–986.

[Bueno et al.(2026)] Anderson S. Bueno, Chase D. Mendenhall, Marina Anciães, Luiz dos Anjos, Víctor Arroyo-Rodríguez, Marco Aurélio-Silva, Cristina Banks-Leite, Matthew G. Betts, Arthur A. Bispo, Andrea Larissa Boesing, Marconi Campos-Cerqueira, Olivier Claessens, Will Cresswell, Gretchen C. Daily, Filibus Danjuma Dami, Sidnei M. Dantas, Pedro F. Develey, Ping Ding, David P. Edwards, Márcio A. Efe, Deborah Faria, Kenneth J. Feeley, Thomas W. Gillespie, Adam S. Hadley, Jack H. Hatfield, Luiza Magalli Pinto Henriques, Lars H. Holbech, Gregory J. Irving, Urs G. Kormann, M. Jyothi Krishnan, Marilise M. Krügel, Jesse R. Lasky, Michael J. Lawes, Alexander C. Lees, Luc Lens, Lahert William Lobo-Araújo, Leithen K. M'Gonigle, Mohammad Saiful Mansor, Shiiwua A. Manu, Miguel Ângelo Marini,

Alexandre Camargo Martensen, Thomas J. Matthews, Jean Paul Metzger, Randall Moore, José Carlos Morante-Filho, P. O. Nameer, Shukor Md Nor, Helon Simões Oliveira, Rômulo Ribon, Viviana Ruiz-Gutiérrez, Luís Fábio Silveira, Philip C Stouffer, John W. Terborgh, Alexandre Uezu, Yanping Wang, Robyn Wethered, Ding Li Yong, and Carlos A. Peres. 2026. High-Quality Surrounding Landscapes Mitigate Avian Extirpations from Forest Remnants. *Proceedings of the National Academy of Sciences* 123, 14 (April 2026), e2521783123. doi:10.1073/pnas.2521783123

[Callaghan et al.(2019)] Corey T. Callaghan, Jodi J. L. Rowley, William K. Cornwell, Alistair G. B. Poore, and Richard E. Major. 2019. Improving Big Citizen Science Data: Moving beyond Haphazard Sampling. *PLOS Biology* 17, 6 (June 2019), e3000357. doi:10.1371/journal.pbio.3000357

[Chase et al.(2020)] Jonathan M. Chase, Shane A. Blowes, Tiffany M. Knight, Katharina Gerstner, and Felix May. 2020. Ecosystem Decay Exacerbates Biodiversity Loss with Habitat Loss. *Nature* 584, 7820 (Aug. 2020), 238–243. doi:10.1038/s41586-020-2531-2

[Chen et al.(2011)] I-Ching Chen, Jane K. Hill, Ralf Ohlemüller, David B. Roy, and Chris D. Thomas. 2011. Rapid Range Shifts of Species Associated with High Levels of Climate Warming. *Science* 333, 6045 (Aug. 2011), 1024–1026. doi:10.1126/science.1206432

[Chetlur et al.(2014)] Sharan Chetlur, Cliff Woolley, Philippe Vandermersch, Jonathan Cohen, John Tran, Bryan Catanzaro, and Evan Shelhamer. 2014. cuDNN: Efficient Primitives for Deep Learning. arXiv:1410.0759 [cs] doi:10.48550/arXiv.1410.0759

[Claramunt et al.(2022)] Santiago Claramunt, Milly Hong, and Adriana Bravo. 2022. The Effect of Flight Efficiency on Gap-Crossing Ability in Amazonian Forest Birds. *Biotropica* 54, 4 (2022), 860–868.

[Convention on Biological Diversity(2022)] Convention on Biological Diversity. 2022. *COP 15 - Report of the Conference of the Parties to the Convention on Biological Diversity on Its Fifteenth Meeting (Part I).* Technical Report.

[Correa Ayram et al.(2016)] Camilo A. Correa Ayram, Manuel E. Mendoza, Andres Etter, and Diego R. Pérez Salicrup. 2016. Habitat Connectivity in Biodiversity Conservation: A Review of Recent Studies and Applications. *Progress in Physical Geography* 40, 1 (2016), 7–37.

[Creech et al.(2024)] Tyler G. Creech, Angela Brennan, Jamie Faselt, Jared A. Stabach, and Annika T. H. Keeley. 2024. Validating Connectivity Models: A Synthesis. *Current Landscape Ecology Reports* 9, 4 (Sept. 2024), 120–134. doi:10.1007/s40823-024-00102-8

[Daniel et al.(2023)] Alexandrine Daniel, Paul Savary, Jean-Christophe Foltête, Aurélie Khimoun, Bruno Faivre, Anthony Ollivier, Cyril Éraud, Hervé Moal, Gilles Vuidel, and Stéphane Garnier. 2023. Validating Graph-based Connectivity Models with Independent Presence–Absence and Genetic Data Sets. *Conservation Biology* 37, 3 (June 2023), e14047. doi:10.1111/cobi.14047

[DeMatteo et al.(2023)] Karen E. DeMatteo, Orlando M. Escalante, Daiana M. Ibañez Alegre, Miguel A. Rinas, Delfina Sotorres, and Carina F. Argüelles. 2023. A Multispecies Corridor in a Fragmented Landscape: Evaluating Effectiveness and Identifying High-Priority Target Areas. *Plos one* 18, 4 (2023), e0283258.

[Dickinson et al.(2010)] Janis L. Dickinson, Benjamin Zuckerberg, and David N. Bonter. 2010. Citizen Science as an Ecological Research Tool: Challenges and Benefits. *Annual Review of Ecology, Evolution, and Systematics* 41, 1 (Dec. 2010), 149–172. doi:10.1146/annurev-ecolsys-102209-144636

[Dickson et al.(2019)] Brett G. Dickson, Christine M. Albano, Ranjan Anantharaman, Paul Beier, Joe Fargione, Tabitha A. Graves, Miranda E. Gray, Kimberly R. Hall, Josh J. Lawler, Paul B. Leonard, Caitlin E. Littlefield, Meredith L. McClure, John Novembre, Carrie A. Schloss, Nathan H. Schumaker, Viral B. Shah, and David M. Theobald. 2019. Circuit-theory Applications to Connectivity Science and Conservation. *Conservation Biology* 33, 2 (April 2019), 239–249. doi:10.1111/cobi.13230

[Fan et al.(2024)] Haiying Fan, Weibin Guo, Buge Lin, Zhiqing Hu, Changcao Wang, and Shaobin Li. 2024. The Influence of Wing Morphology upon Intraspecific Divergence in Birds: A Global Study of Subspecies Richness. *Avian Research* 15 (2024), 100188.

[Farley et al.(2018)] Scott S Farley, Andria Dawson, Simon J Goring, and John W Williams. 2018. Situating Ecology as a Big-Data Science: Current Advances, Challenges, and Solutions. *BioScience* 68, 8 (Aug. 2018), 563–576. doi:10.1093/biosci/biy068

[Fletcher et al.(2023)] Robert J. Fletcher, Maria E. Iezzi, Robert Guralnick, Andrew J. Marx, Sadie J. Ryan, and Denis Valle. 2023. A Framework for Linking Dispersal Biology to Connectivity across Landscapes. *Landscape Ecology* 38, 10 (Oct. 2023), 2487–2500. doi:10.1007/s10980-023-01741-8

[Fletcher et al.(2024)] Robert J. Fletcher, Thomas A.H. Smith, Savannah Troy, Nicholas Kortessis, Edgar C. Turner, Emilio M. Bruna, and Robert D. Holt. 2024. The Prominent Role of the Matrix in Ecology, Evolution, and Conservation. *Annual Review of Ecology, Evolution, and Systematics* 55, 1 (Nov. 2024), 423–447. doi:10.1146/annurev-ecolsys-102722-025653

[Fletcher Jr. et al.(2019)] Robert J. Fletcher Jr., Jorge A. Sefair, Chao Wang, Caroline L. Poli, Thomas A. H. Smith, Emilio M. Bruna, Robert D. Holt, Michael Barfield, Andrew J. Marx, and Miguel A. Acevedo. 2019. Towards a Unified Framework for Connectivity That Disentangles Movement and Mortality in Space and Time. *Ecology Letters* 22, 10 (2019), 1680–1689. useful paper that links dispersal to demographic processes via spatially-explicitly measuring mortality risk. doi:10.1111/ele.13333

[Fraser et al.(2018)] Kevin C. Fraser, Kimberley TA Davies, Christina M. Davy, Adam T. Ford, D. T. Flockhart, and Eduardo G. Martins. 2018. Tracking the Conservation Promise of Movement Ecology. *Frontiers in Ecology and Evolution* 6 (2018), 150.

[Fredston et al.(2025)] Alexa L. Fredston, Morgan W. Tingley, Montague HC Neate-Clegg, Luke J. Evans, Laura H. Antão, Natalie C. Ban, I.-Ching Chen, Yi-Wen Chen, Lise Comte, and David P. Edwards. 2025. Reimagining Species on the Move across Space and Time. *Trends in ecology & evolution* (2025).

[Gillies and St. Clair(2010)] Cameron S. Gillies and Colleen Cassady St. Clair. 2010. Functional Responses in Habitat Selection by Tropical Birds Moving through Fragmented Forest. *Journal of Applied Ecology* 47, 1 (Feb. 2010), 182–190. doi:10.1111/j.1365-2664.2009.01756.x

[Grass et al.(2019)] Ingo Grass, Jacqueline Loos, Svenja Baensch, Péter Batáry, Felipe Librán-Embid, Anoush Ficiciyan, Felix Klaus, Maraja Riechers, Julia Rosa, Julia Tiede, Kristy Udy, Catrin Westphal, Annemarie Wurz, and Teja Tscharntke. 2019. Land-sharing/-sparing Connectivity Landscapes for Ecosystem Services and Biodiversity Conservation. *People and Nature* 1, 2 (June 2019), 262–272. doi:10.1002/pan3.21

[Greenwood and Harvey(1982)] Paul J. Greenwood and Paul H. Harvey. 1982. The Natal and Breeding Dispersal of Birds. *Annual review of ecology and systematics* 13 (1982), 1–21. jstor:2097060

[Hall et al.(2021)] Kimberly R. Hall, Ranjan Anantharaman, Vincent A. Landau, Melissa Clark, Brett G. Dickson, Aaron Jones, Jim Platt, Alan Edelman, and Viral B. Shah. 2021. Circuitscape in Julia: Empowering Dynamic Approaches to Connectivity Assessment. *Land* 10, 3 (March 2021), 301. doi:10.3390/land10030301

[Hanski(1998)] Ilkka Hanski. 1998. Metapopulation Dynamics. *Nature* 396, 6706 (Nov. 1998), 41–49. Very important paper to cite on metapopulation and extinction-colonization dynamics.. doi:10.1038/23876

[Heller and Zavaleta(2009)] Nicole E. Heller and Erika S. Zavaleta. 2009. Biodiversity Management in the Face of Climate Change: A Review of 22 Years of Recommendations. *Biological Conservation* 142, 1 (Jan. 2009), 14–32. doi:10.1016/j.biocon.2008.10.006

[Hofmann et al.(2023)] David D. Hofmann, Gabriele Cozzi, John W. McNutt, Arpat Ozgul, and Dominik M. Behr. 2023. A Three-Step Approach for

Assessing Landscape Connectivity via Simulated Dispersal: African Wild Dog Case Study. *Landscape Ecology* 38, 4 (April 2023), 981–998. doi:10.1007/s10980-023-01602-4

[IUCN(2023)] IUCN. 2023. Habitats Classification Scheme (Version 3.1).

[James et al.(2021)] Tamora D. James, Roberto Salguero-Gómez, Owen R. Jones, Dylan Z. Childs, and Andrew P. Beckerman. 2021. Bridging Gaps in Demographic Analysis with Phylogenetic Imputation. *Conservation Biology* 35, 4 (Aug. 2021), 1210–1221. doi:10.1111/cobi.13658

[Jennings et al.(2020)] Megan K. Jennings, Emily Haeuser, Diane Foote, Rebecca L. Lewison, and Erin Conlisk. 2020. Planning for Dynamic Connectivity: Operationalizing Robust Decision-Making and Prioritization Across Landscapes Experiencing Climate and Land-Use Change. *Land* 9, 10 (Oct. 2020), 341. connectivity and climate change. doi:10.3390/land9100341

[Johnston et al.(2021)] Alison Johnston, Wesley M. Hochachka, Matthew E. Strimas-Mackey, Viviana Ruiz Gutierrez, Orin J. Robinson, Eliot T. Miller, Tom Auer, Steve T. Kelling, and Daniel Fink. 2021. Analytical Guidelines to Increase the Value of Community Science Data: An Example Using eBird Data to Estimate Species Distributions. *Diversity and Distributions* 27, 7 (July 2021), 1265–1277. doi:10.1111/ddi.13271

[Jung et al.(2020)] Martin Jung, Prabhat Raj Dahal, Stuart H. M. Butchart, Paul F. Donald, Xavier De Lamo, Myroslava Lesiv, Valerie Kapos, Carlo Rondinini, and Piero Visconti. 2020. A Global Map of Terrestrial Habitat Types. doi:10.5281/ZENODO.4058819

[Koen et al.(2014)] Erin L. Koen, Jeff Bowman, Carrie Sadowski, and Aaron A. Walpole. 2014. Landscape Connectivity for Wildlife: Development and Validation of Multispecies Linkage Maps. *Methods in Ecology and Evolution* 5, 7 (July 2014), 626–633. doi:10.1111/2041-210X.12197

[La Sorte et al.(2020)] Frank A. La Sorte, Myla FJ Aronson, Christopher A. Lepczyk, and Kyle G. Horton. 2020. Area Is the Primary Correlate of Annual and Seasonal Patterns of Avian Species Richness in Urban Green Spaces. *Landscape and Urban Planning* 203 (2020), 103892.

[La Sorte et al.(2024)] Frank A. La Sorte, Jeremy M. Cohen, and Walter Jetz. 2024. Data Coverage, Biases, and Trends in a Global Citizen-science Resource for Monitoring Avian Diversity. *Diversity and Distributions* 30, 8 (Aug. 2024), e13863. doi:10.1111/ddi.13863

[La Sorte and Somveille(2020)] Frank A. La Sorte and Marius Somveille. 2020. Survey Completeness of a Global Citizen-Science Database of Bird Occurrence. *Ecography* 43, 1 (2020), 34–43. doi:10.1111/ecog.04632

[Landau et al.(2021)] Vincent Landau, Viral Shah, Ranjan Anantharaman, and Kimberly Hall. 2021. Omniscape.Jl: Software to Compute Omnidirectional Landscape Connectivity. *Journal of Open Source Software* 6, 57 (Jan. 2021), 2829. doi:10.21105/joss.02829

[Liczner et al.(2024)] Amanda R. Liczner, Richard Pither, Joseph R. Bennett, Jeff Bowman, Kimberly R. Hall, Robert J. Fletcher, Adam T. Ford, Julia L. Michalak, Bronwyn Rayfield, Julian Wittische, and Jason Pither. 2024. Advances and Challenges in Ecological Connectivity Science. *Ecology and Evolution* 14, 9 (Sept. 2024), e70231. doi:10.1002/ece3.70231

[Littlefield et al.(2019)] Caitlin E. Littlefield, Meade Krosby, Julia L. Michalak, and Joshua J. Lawler. 2019. Connectivity for Species on the Move: Supporting Climate-driven Range Shifts. *Frontiers in Ecology and the Environment* 17, 5 (2019), 270–278.

[Lomolino(2000)] Mark V. Lomolino. 2000. Ecology's Most General, yet Protean Pattern: The Species-Area Relationship. *Journal of biogeography* (2000), 17–26. jstor:2655979

[Manning et al.(2006)] Adrian D. Manning, Joern Fischer, and David B. Lindenmayer. 2006. Scattered Trees Are Keystone Structures–Implications for Conservation. *Biological conservation* 132, 3 (2006), 311–321.

[Martensen et al.(2012)] Alexandre Camargo Martensen, Milton Cezar Ribeiro, Cristina Banks-Leite, Paulo Inácio Prado, and Jean Paul Metzger. 2012. Associations of Forest Cover, Fragment Area, and Connectivity with Neotropical Understory Bird Species Richness and Abundance. *Conservation Biology* 26, 6 (Dec. 2012), 1100–1111. doi:10.1111/j.1523-1739.2012.01940.x

[Martin(2001)] Thomas E. Martin. 2001. Abiotic Vs. Biotic Influences on Habitat Selection of Coexisting Species: Climate Change Impacts? *Ecology* 82, 1 (2001), 175–188. doi:10.1890/0012-9658(2001)082[0175:AVBIOH]2.0.CO;2

[Mateo-Sánchez et al.(2015)] Maria C. Mateo-Sánchez, Niko Balkenhol, Sam Cushman, Trinidad Pérez, Ana Domínguez, and Santiago Saura. 2015. Estimating Effective Landscape Distances and Movement Corridors: Comparison of Habitat and Genetic Data. *Ecosphere* 6, 4 (2015), 1–16.

[McClure et al.(2016)] Meredith L. McClure, Andrew J. Hansen, and Robert M. Inman. 2016. Connecting Models to Movements: Testing Connectivity Model Predictions against Empirical Migration and Dispersal Data. *Landscape Ecology* 31, 7 (Sept. 2016), 1419–1432. doi:10.1007/s10980-016-0347-0

[McGuire et al.(2016)] Jenny L. McGuire, Joshua J. Lawler, Brad H. McRae, Tristan A. Nuñez, and David M. Theobald. 2016. Achieving Climate Connectivity in a Fragmented Landscape. *Proceedings of the National Academy of Sciences* 113, 26 (2016), 7195–7200.

[McRae et al.(2016)] Brad McRae, K. Popper, A. Jones, M. Schindel, S. Buttrick, K. Hall, R.S. Unnasch, and J. Platt. 2016. *Conserving Nature's Stage: Mapping Omnidirectional Connectivity for Resilient Terrestrial Landscapes in the Pacific Northwest.* Technical Report. The Nature Conservancy.

[McRae and Beier(2007)] Brad H. McRae and Paul Beier. 2007. Circuit Theory Predicts Gene Flow in Plant and Animal Populations. *Proceedings of the National Academy of Sciences* 104, 50 (2007), 19885–19890.

[McRae et al.(2008)] Brad H. McRae, Brett G. Dickson, Timothy H. Keitt, and Viral B. Shah. 2008. Using Circuit Theory to Model Connectivity in Ecology, Evolution, and Conservation. *Ecology* 89, 10 (2008), 2712–2724. doi:10.1890/07-1861.1

[McRae and Kavanagh(2011)] Brad H. McRae and Darren M. Kavanagh. 2011. Linkage Mapper Connectivity Analysis Software. *The Nature Conservancy, Seattle WA* (2011).

[Minor and Urban(2008)] Emily S. Minor and Dean L. Urban. 2008. A Graph-Theory Framework for Evaluating Landscape Connectivity and Conservation Planning. *Conservation Biology* 22, 2 (2008), 297–307. doi:10.1111/j.1523-1739.2007.00871.x

[Mishra et al.(2018)] Abhishek Mishra, Sudipta Tung, P. M. Shreenidhi, Mohammed Aamir Sadiq, V. R. Shree Sruti, Partha Pratim Chakraborty, and Sutirth Dey. 2018. Sex Differences in Dispersal Syndrome Are Modulated by Environment and Evolution. *Philosophical Transactions of the Royal Society B: Biological Sciences* 373, 1757 (Aug. 2018), 20170428. doi:10.1098/rstb.2017.0428

[Moilanen(2011)] Atte Moilanen. 2011. On the Limitations of Graph-Theoretic Connectivity in Spatial Ecology and Conservation. *Journal of Applied Ecology* 48, 6 (2011), 1543–1547. jstor:41318990

[Molina-Venegas(2024)] Rafael Molina-Venegas. 2024. How to Get the Most out of Phylogenetic Imputation without Abusing It. *Methods in Ecology and Evolution* 15, 3 (March 2024), 456–463. doi:10.1111/2041-210X.14198

[Montes-Rojas et al.(2024)] Andrés Montes-Rojas, Nicolás Alejandro José Delgado-Morales, Rafael S. Escucha, Laura C. Siabatto, and Andrés Link. 2024. Recovering Connectivity through Restoration Corridors in a Fragmented Landscape in the Magdalena River's Valley in Colombia. *Biodiversity and Conservation* 33, 11 (Sept. 2024), 3171–3185. doi:10.1007/s10531-024-02907-9

[Olds et al.(2012)] Andrew D. Olds, Rod M. Connolly, Kylie A. Pitt, and Paul S. Maxwell. 2012. Habitat Connectivity Improves Reserve Performance. *Conservation Letters* 5, 1 (Jan. 2012), 56–63. doi:10.1111/j.1755-263X.2011.00204.x

[Panzacchi et al.(2016)] Manuela Panzacchi, Bram Van Moorter, Olav Strand, Marco Saerens, Ilkka Kivimäki, Colleen C. St. Clair, Ivar Herfindal, and Luigi Boitani. 2016. Predicting the Continuum between Corridors and Barriers to Animal Movements Using Step Selection Functions and Randomized Shortest Paths. *Journal of Animal Ecology* 85, 1 (2016), 32–42. methods for mammals in modeling connectivity (RSF's).

[Paradis et al.(2002)] Emmanuel Paradis, Stephen R. Baillie, and William J. Sutherland. 2002. Modeling Large-Scale Dispersal Distances. *Ecological Modelling* 151, 2-3 (2002), 279–292.

[Paszke et al.(2019)] Adam Paszke, Sam Gross, Francisco Massa, Adam Lerer, James Bradbury, Gregory Chanan, Trevor Killeen, Zeming Lin, Natalia Gimelshein, and Luca Antiga. 2019. Pytorch: An Imperative Style, High-Performance Deep Learning Library. *Advances in neural information processing systems* 32 (2019).

[Phillips et al.(2021)] Payton Phillips, Melissa M. Clark, Suraj Baral, Erin L. Koen, and Jeff Bowman. 2021. Comparison of Methods for Estimating Omnidirectional Landscape Connectivity. *Landscape Ecology* 36, 6 (June 2021), 1647–1661. doi:10.1007/s10980-021-01254-2

[Pither et al.(2023)] Richard Pither, Paul O'Brien, Angela Brennan, Kristen Hirsh-Pearson, and Jeff Bowman. 2023. Predicting Areas Important for Ecological Connectivity throughout Canada. *PLoS One* 18, 2 (2023), e0281980.

[Prugh et al.(2008)] Laura R. Prugh, Karen E. Hodges, Anthony R. E. Sinclair, and Justin S. Brashares. 2008. Effect of Habitat Area and Isolation on Fragmented Animal Populations. *Proceedings of the National Academy of Sciences* 105, 52 (Dec. 2008), 20770–20775. doi:10.1073/pnas.0806080105

[Pullinger and Johnson(2010)] Michael G. Pullinger and Chris J. Johnson. 2010. Maintaining or Restoring Connectivity of Modified Landscapes: Evaluating the Least-Cost Path Model with Multiple Sources of Ecological Information. *Landscape Ecology* 25 (2010), 1547–1560.

[Rayfield et al.(2011)] Bronwyn Rayfield, Marie-Josée Fortin, and Andrew Fall. 2011. Connectivity for Conservation: A Framework to Classify Network Measures. *Ecology* 92, 4 (2011), 847–858.

[Richard and Armstrong(2010)] Yvan Richard and Doug P. Armstrong. 2010. Cost Distance Modelling of Landscape Connectivity and Gap-Crossing Ability Using Radio-Tracking Data: Cost Distance Modelling of Landscape Connectivity. *Journal of Applied Ecology* 47, 3 (April 2010), 603–610. doi:10.1111/j.1365-2664.2010.01806.x

[Rushing et al.(2015)] Clark S. Rushing, Michele R. Dudash, Colin E. Studds, and Peter P. Marra. 2015. Annual Variation in Long-Distance Dispersal Driven by Breeding and Non-Breeding Season Climatic Conditions in a Migratory Bird. *Ecography* 38, 10 (2015), 1006–1014. doi:10.1111/ecog.01196

[Saura et al.(2011)] Santiago Saura, Christine Estreguil, Coralie Mouton, and Mónica Rodríguez-Freire. 2011. Network Analysis to Assess Landscape Connectivity Trends: Application to European Forests (1990–2000). *Ecological Indicators* 11, 2 (2011), 407–416.

[Saura and Torné(2009)] Santiago Saura and Josep Torné. 2009. Conefor Sensinode 2.2: A Software Package for Quantifying the Importance of Habitat Patches for Landscape Connectivity. *Environmental modelling & software* 24, 1 (2009), 135–139.

[Şekercioğlu et al.(2025)] Çağan H. Şekercioğlu, Kyle D. Kittelberger, Flavio MM Mota, Amy N. Buxton, Nikolas Orton, Adara DeNiro, Evan R. Buechley, Joshua J. Horns, Judson D. Blount, and Jason Socci. 2025. BIRDBASE: A Global Dataset of Avian Biogeography, Conservation, Ecology and Life History Traits. *Scientific Data* 12, 1 (2025), 1558.

[Shaw et al.(2025)] Robyn E. Shaw, Katherine A. Farquharson, Michael W. Bruford, David J. Coates, Carole P. Elliott, Joachim Mergeay, Kym M. Ottewell, Gernot Segelbacher, Sean Hoban, Christina Hvilsom, Sílvia Pérez-Espona, Dainis Ruņģis, Filippos Aravanopoulos, Laura D. Bertola, Helena Cotrim, Karen Cox, Vlatka Cubric-Curik, Robert Ekblom, José A. Godoy, Maciej K. Konopiński, Linda Laikre, Isa-Rita M. Russo, Nevena Veličković, Philippine Vergeer, Carles Vilà, Vladimir Brajkovic, David L. Field, William P. Goodall-Copestake, Frank Hailer, Tara Hopley, Frank E. Zachos, Paulo C. Alves, Aleksandra Biedrzycka, Rachel M. Binks, Joukje Buiteveld, Elena Buzan, Margaret Byrne, Barton Huntley, Laura Iacolina, Naomi L. P. Keehnen, Peter Klinga, Alexander Kopatz, Sara Kurland, Jennifer A. Leonard, Chiara Manfrin, Alexis Marchesini, Melissa A. Millar, Pablo Orozco-terWengel, Jente Ottenburghs, Diana Posledovich, Peter B. Spencer, Nikolaos Tourvas, Tina Unuk Nahberger, Pim van Hooft, Rita Verbylaite, Cristiano Vernesi, and Catherine E. Grueber. 2025. Global Meta-Analysis Shows Action Is Needed to Halt Genetic Diversity Loss. *Nature* (Jan. 2025), 1–7. doi:10.1038/s41586-024-08458-x

[Sheard et al.(2020)] Catherine Sheard, Montague HC Neate-Clegg, Nico Alioravainen, Samuel EI Jones, Claire Vincent, Hannah EA MacGregor, Tom P. Bregman, Santiago Claramunt, and Joseph A. Tobias. 2020. Ecological Drivers of Global Gradients in Avian Dispersal Inferred from Wing Morphology. *Nature communications* 11, 1 (2020), 2463.

[Simberloff and Abele(1982)] Daniel Simberloff and Lawrence G. Abele. 1982. Refuge Design and Island Biogeographic Theory: Effects of Fragmentation. *The American Naturalist* 120, 1 (July 1982), 41–50. doi:10.1086/283968

[Spanowicz and Jaeger(2019)] Ariel G. Spanowicz and Jochen A. G. Jaeger. 2019. Measuring Landscape Connectivity: On the Importance of within-Patch Connectivity. *Landscape Ecology* 34, 10 (Oct. 2019), 2261–2278. doi:10.1007/s10980-019-00881-0

[Sullivan et al.(2009)] Brian L. Sullivan, Christopher L. Wood, Marshall J. Iliff, Rick E. Bonney, Daniel Fink, and Steve Kelling. 2009. eBird: A Citizen-Based Bird Observation Network in the Biological Sciences. *Biological conservation* 142, 10 (2009), 2282–2292.

[Tabor et al.(2025)] Karyn M. Tabor, Natasha Stavros, Dawn Biehler, Liliana C. Castillo-Villamor, Dillon Mahmoudi, Luis Mario Moreno Amado, and Margaret B. Holland. 2025. Digital Equity in a Crowded Tool Space: Navigating Opportunities and Challenges for Equitable Implementation of Conservation Technologies. *Conservation Science and Practice* 7, 1 (Jan. 2025), e13279. doi:10.1111/csp2.13279

[Taylor et al.(1993)] Philip D. Taylor, Lenore Fahrig, Kringen Henein, and Gray Merriam. 1993. Connectivity Is a Vital Element of Landscape Structure. *Oikos* (1993), 571–573.

[Tischendorf and Fahrig(2000)] Lutz Tischendorf and Lenore Fahrig. 2000. How Should We Measure Landscape Connectivity? *Landscape ecology* 15, 7 (2000), 633–641.

[Tobias et al.(2022)] Joseph A. Tobias, Catherine Sheard, Alex L. Pigot, Adam JM Devenish, Jingyi Yang, Ferran Sayol, Montague HC Neate-Clegg, Nico Alioravainen, Thomas L. Weeks, and Robert A. Barber. 2022. AVONET: Morphological, Ecological and Geographical Data for All Birds. *Ecology Letters* 25, 3 (2022), 581–597.

[Unnithan Kumar and Cushman(2022)] Siddharth Unnithan Kumar and Samuel A. Cushman. 2022. Connectivity Modelling in Conservation Science: A Comparative Evaluation. *Scientific Reports* 12, 1 (2022), 16680.

[Urban and Keitt(2001)] Dean Urban and Timothy Keitt. 2001. Landscape Connectivity: A Graph-Theoretic Perspective. *Ecology* 82, 5 (2001), 1205–1218.

[Ward et al.(2020)] Michelle Ward, Santiago Saura, Brooke Williams, Juan Pablo Ramírez-Delgado, Nur Arafeh-Dalmau, James R. Allan, Oscar Venter, Grégoire Dubois, and James EM Watson. 2020. Just Ten Percent of the Global Terrestrial Protected Area Network Is Structurally Connected via Intact Land. *Nature communications* 11, 1 (2020), 4563.

[Watling et al.(2011)] James I. Watling, A. Justin Nowakowski, Maureen A. Donnelly, and John L. Orrock. 2011. Meta-Analysis Reveals the Importance of Matrix Composition for Animals in Fragmented Habitat: Connectivity Meta-Analysis. *Global Ecology and Biogeography* 20, 2 (March 2011), 209–217. doi:10.1111/j.1466-8238.2010.00586.x

[Watson et al.(2018)] James E. M. Watson, Tom Evans, Oscar Venter, Brooke Williams, Ayesha Tulloch, Claire Stewart, Ian Thompson, Justina C. Ray, Kris Murray, Alvaro Salazar, Clive McAlpine, Peter Potapov, Joe Walston, John G. Robinson, Michael Painter, David Wilkie, Christopher Filardi, William F. Laurance, Richard A. Houghton, Sean Maxwell, Hedley Grantham, Cristián Samper, Stephanie Wang, Lars Laestadius, Rebecca K. Runting, Gustavo A. Silva-Chávez, Jamison Ervin, and David Lindenmayer. 2018. The Exceptional Value of Intact Forest Ecosystems. *Nature Ecology & Evolution* 2, 4 (April 2018), 599–610. doi:10.1038/s41559-018-0490-x

[Weeks et al.(2022)] Brian C. Weeks, Bruce K. O'Brien, Jonathan J. Chu, Santiago Claramunt, Catherine Sheard, and Joseph A. Tobias. 2022. Morphological Adaptations Linked to Flight Efficiency and Aerial Lifestyle Determine Natal Dispersal Distance in Birds. *Functional Ecology* 36, 7 (July 2022), 1681–1689. doi:10.1111/1365-2435.14056

[Wikelski et al.(2007)] Martin Wikelski, Roland W. Kays, N. Jeremy Kasdin, Kasper Thorup, James A. Smith, and George W. Swenson Jr. 2007. Going Wild: What a Global Small-Animal Tracking System Could Do for Experimental Biologists. *Journal of Experimental Biology* 210, 2 (2007), 181–186.

[Wintle et al.(2019)] Brendan A. Wintle, Heini Kujala, Amy Whitehead, Alison Cameron, Sam Veloz, Aija Kukkala, Atte Moilanen, Ascelin Gordon, Pia E. Lentini, Natasha C. R. Cadenhead, and Sarah A. Bekessy. 2019. Global Synthesis of Conservation Studies Reveals the Importance of Small Habitat Patches for Biodiversity. *Proceedings of the National Academy of Sciences* 116, 3 (Jan. 2019), 909–914. doi:10.1073/pnas.1813051115

[Wood et al.(2022)] Sylvia L. R. Wood, Kyle T. Martins, Véronique Dumais-Lalonde, Olivier Tanguy, Fanny Maure, Annick St-Denis, Bronwyn Rayfield, Amanda E. Martin, and Andrew Gonzalez. 2022. Missing Interactions: The Current State of Multispecies Connectivity Analysis. *Frontiers in Ecology and Evolution* 10 (2022).

[Zeller et al.(2018)] Katherine A. Zeller, Megan K. Jennings, T. Winston Vickers, Holly B. Ernest, Samuel A. Cushman, and Walter M. Boyce. 2018. Are All Data Types and Connectivity Models Created Equal? Validating Common Connectivity Approaches with Dispersal Data. *Diversity and Distributions* 24, 7 (2018), 868–879. comparing methods of generating resistance layers for mammal connectivity. doi:10.1111/ddi.12742

[Zou et al.(2025)] Yibiao Zou, Thomas W. Crowther, Gabriel Reuben Smith, Haozhi Ma, Lidong Mo, Lalasia Bialic-Murphy, Peter Potapov, Klementyna A. Gawecka, Chi Xu, Pablo J. Negret, Thomas Lauber, Zhaofei Wu, Dominic Rebindaine, and Constantin M. Zohner. 2025. Fragmentation Increased in over Half of Global Forests from 2000 to 2020. *Science* 389, 6765 (Sept. 2025), 1151–1156. doi:10.1126/science.adr6450

[Zurell et al.(2025)] Damaris Zurell, Greta Bocedi, Santiago J. E. Velazco, Andrew Gonzalez, Andy Purvis, Brendan Wintle, Cory Merow, Carolyn Lundquist, Gurutzeta Guillera-Arroita, Josef Settele, Josep M. Serra-Diaz, Juliano Sarmento Cabral, Justin M. J. Travis, Katrin Schifferle, Lauren Buckley, Natalie J. Briscoe, Nick J. B. Isaac, Pedro R. Peres-Neto, Raya Keuth, Samuel J. L. Gascoigne, Simon Ferrier, and Mark C. Urban. 2025. Predicting the Way Forward for the Global Biodiversity Framework. *Proceedings of the National Academy of Sciences* 122, 41 (Oct. 2025), e2501695122. doi:10.1073/pnas.2501695122

Supplementary Information

S1 EcoScape Algorithm Details

S1.1 Flow Computation

The flow f_{ij} through pixel ij represents the amount of repopulation due to dispersal paths through pixel ij. To compute, we multiply the permeability by the gradient of FCH (the fully connected habitat) with respect to permeability:

$$f_{ij} = p_{ij} \frac{\partial \mathrm{FCH}}{\partial p_{ij}} \,. \tag{2}$$

The flow is computed via the gradient back-propagation mechanism of machine-learning framework such as PyTorch. To this end, FCH is considered as the model output, and p as the input. The gradient back-propagation of the output with respect to the inputs yields $\partial \mathrm{FCH}/\partial p$, and the flow can be obtained by multiplying the result by the permeability layer. This allows for fast, GPU-accelerated computation of the flow.

To prove that (2) indeed computes the contribution of pixel ij to repopulation due to dispersal paths that go through ij, we need to carefully consider the dispersal simulation, tracking the paths used for dispersal in each simulation.

Let $r^{(0)}$ be the repopulation layer after seed initialization, and let $r^{(m)}$ be the layer after the m-th iteration of (1), so that (1) can be rewritten as

$$r_{ij}^{m+1} := \max\left\{ r_{ij}^{m},\ X_{ij} \cdot p_{ij} \cdot \max_{kl \in N(ij)} \left(Y_{kl} \cdot r_{kl}^{m} \right) \right\} \,. \tag{3}$$

Then, it is easy to see that the sequence $r^{(0)}, r^{(1)}, r^{(2)}, \ldots$ is monotonically increasing, so that at each ij, $r_{ij}^{(0)} \le r_{ij}^{(1)} \le r_{ij}^{(2)} \le \cdots$.

To track where the repopulation came from, we can define a *source mapping* S, so that the repopulation at pixel ij came from neighboring pixel $S(ij)$. We define this mapping as follows. Initially, $S(ij) = \perp$ at all ij, where $\perp$ is a special symbol indicating that the source is undefined (the population did not come from another location). When we update the value at ij, that is, when $r_{ij}^{(m)} < r_{ij}^{(m+1)}$, there is a unique neighbor $kl \in N(ij)$ that provides the argmax in (3): this kl can be thought of as the *source* of the increased bird population at ij, and therefore, we set $S(ij) := kl$. When the value at ij is unchanged, we leave $S(ij)$ unchanged.

The source mapping S defines a graph, with an edge from ij to kl when $S(ij) = kl$. It is easy to see that this graph is a collection of trees, each tree having root in a repopulation seed. Indeed, there can be no loops in the graph: $S(ij) = kl$ implies $r_{ij}^{(m+1)} < r_{kl}^{(m)}$ at the time $m+1$ of the last update of kl, and by monotonicity, $r_{ij}^{(n)} < r_{kl}^{(n)}$ after the last update n. Thus, the EcoScape algorithm can be understood as a way to generate random dispersal trees rooted in the repopulation seeds. This alternate characterization is essential to the computation of the flow layer. Finally, the connectivity layer

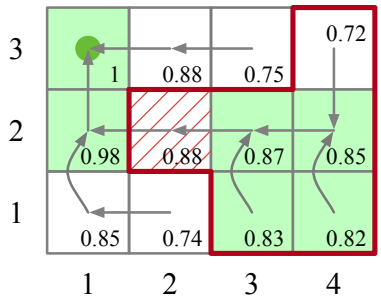

Supp. Figure S1. A repopulation layer r. The value r_{ij} is indicated in each pixel ij; pixel in the habitat are depicted in green, and pixel $(1,3)$ is the (only) seed, with $r_{1,3} = 1$. The source mapping S is depicted with arrows: for instance, we have $S(1,2) = (1,3)$ (pixel $(1,2)$ points to the sink $(1,3)$) and $S(2,2) = (1,2)$. We note that the arrows point from cell to population source, and are thus oriented in the opposite direction of those of Figure 2. Pixel $(2,2)$ is highlighted with red cross-hatching, and its downstream region $U(2,2) = \{(2,2),(3,1),(3,2),(4,1),(4,2),(4,3)\}$ is shown with a bold red border. We have $f_{2,2} = 0.87 + 0.85 + 0.83 + 0.82 = 3.37$, so that the flow at $(2,2)$ corresponds to the habitat repopulation that flowed through $(2,2)$.

is obtained by clipping the repopulation to the habitat via $c = h\, r^{(n)}$, where multiplication is pixel-wise.

The flow at a pixel indicates how much of the connectivity is due to movement through the pixel. To see this, let $c_{ij} = c_{ij}^{(n)}$ be the connectivity, and let S be the source mapping defined above. The locations that owe their repopulation to ij consists of ij, its immediate descendants in the propagation trees, or the kl with $S(kl) = ij$, and their descendants of any level: we call this the *downstream region* of ij (see Supp. Figure S1). Precisely, the downstream region of ij is the set of pixels $U(ij)$ that have a path in the graph S to ij. Pixels in $U(ij)$ were repopulated through ij.

If we change the permeability p_{ij} of ij by a small amount δ (small, so as not to change the source mapping), the connectivity in the downstream region of ij will change correspondingly, by $\delta(\partial \mathrm{FCH}/\partial p_{ij})$, where $\mathrm{FCH} = a \sum_{ij} c_{ij}$. If we keep S fixed, that is, if we fix the flow taken by the updates (3), the total habitat repopulation of the downstream region of ij is $p_{ij}(\partial \mathrm{FCH}/\partial p_{ij})$, or:

$$f_{ij} = a \sum_{kl \in U(ij)} c_{kl} = p_{ij} \frac{\partial \mathrm{FCH}}{\partial p_{ij}} \,. \tag{4}$$

This proves (2).

S1.2 Coin Tosses and Random Dispersal Paths

The coin toss in the main repopulation formula update (3) serves the purpose of randomizing the paths taken by species

propagation in each simulation. In Supp. Figure S2, we compare the propagation from a central pixel when coin toss is used (A), or not used so that propagation can always occur, (B). As we see in (B), with no coin toss, repopulation from a pixel can always propagate to the 8 neighboring pixels. This produces a deterministic, and rather unnatural, pattern where in n rounds, a perfectly square region of edge $2n+1$ is repopulated. If coin tosses are used (A), the reachable region is more approximately circular. The corners can be reached only if the n coin tosses along the diagonals all yielded heads, which occurs with the very low probability of 2^{-n}. On the other hand, there are many more ways of reaching up, down, left, and right, since diagonal movements are also permitted. This yields a better approximation to circular propagation, even though the simulation occurs on a square lattice.

The use of coin tosses is also instrumental in obtaining a realistic, multi-path estimation of the flow. In computing the flow, each pixel attributes its repopulation to the pixel that caused the repopulation to increase (formally, to the pixel that realized the argmax in (3). Absent the coin tosses, the propagation to diagonal pixels would be responsible for more flow than propagation to the edge-adjacent (laterally or vertically) pixels. In fact, diagonal propagation gives access to 5 more possible propagation directions in the next simulation step, while edge-adjacent propagation gives access to only 3, as depicted in Supp. Figure S3. The coin toss randomizes whether edge-adjacent, or diagonal, pixels are reached first by the dispersal, improving the modeling of multi-path dispersal. Circuit-based tools such as Omniscape can achieve multi-path modeling and circular symmetry of dispersal without having to resort to coin tosses. The circuit equations naturally lead multi-path propagation, modeling the way current spreads in the square resistor mesh. For uniform resistance, the current pattern has circular symmetry, in spite of the underlying grid being square.

The coin toss needs to be used jointly with the rule that update (3) is applied *only* when $r_{ij}^{m+1} > r_{ij}^{m} + 0.05$. The 0.05 threshold ensures that once a propagation path is chosen, it is not subsequently randomly changed via other argmax applications, which would tend again, in the long run, to favor diagonals. This phenomenon is clearly illustrated in Supp. Figure S4, which compares the flow in the synthetic landscape of Section 2.1.5 that is obtained with the standard computation using (A) the coin toss and 0.05 update threshold, (B) the coin toss but not the update threshold, and (C) the update threshold but not the coin toss.

S1.3 Functionally Connected Habitat and ECA

We develop here a more in-depth connection between the notion of *Functionally Connected Habitat* (FCH), and the *Equivalent Connected Area* (ECA) of [Saura et al.(2011)]. Consider habitat patches $H_1, \ldots, H_n$ with areas A_k, $1 \le k \le n$. Assume as a simplification that the probability with which a bird can propagate via dispersal from a patch H_k to patch H_l is equal to P_{kl}, and is independent on the precise source and destination locations in the patches.

EcoScape computes repopulation simulating dispersal from seeds. Since seeds are placed in the habitat at random, a seed occurs in patch H_k with probability proportional to A_k. Further, a seed in H_k can reach H_l and repopulate it with probability P_{kl} (again using our simplification in which all locations in the same patch are equivalent). As there are A_l pixels in H_l, seeds in H_k generate a total repopulation of H_l equal to $A_k p_{kl} A_l$. Taking into account all source patches H_k, $1 \le k \le n$, the total repopulation of H_l will be proportional to $\sum_{k=1}^{n} A_k p_{kl} A_l$. Summing over all repopulated patches, the total repopulation of the habitat will be

$$\mathrm{FCH} = \sum_{l=1}^{n} \sum_{k=1}^{n} A_k p_{kl} A_l \ ,$$

which is the same formula as the one defining the ECA.

S1.4 Landscape Matrix Permeability

To produce the landscape permeability raster for a species, we start from the species habitat preferences given in the IUCN Red List. For each species, this dataset provides the lists of “major importance" and “suitable" land cover types. We produce a preliminary assignment $\tilde{p}$ of permeability to land cover classes as follows. We assign permeability $\tilde{p}_i = 1$ (no resistance) to land cover types i that are listed as major importance for the species or correspond to forest in the case of forest-specialists. We assign permeability $\tilde{p}_i = 0.9$ to land cover types i that are listed as suitable for the species. All other land cover types i are assigned permeability $\tilde{p}_i = 0$.

We then use eBird data to refine this initial parameter, assigning higher permeability to non-habitat, non-forest land cover types where the species is often observed. We perform the adjustment as follows. We consider all the grid cells associated with eBird checklists occurring in US states that intersect the ranges of the three bird species considered. Precisely, for each species, we consider all eBird grid cells occurring in the following states:

- Acorn Woodpecker: AZ, CA, NM, NV, OR.
- Steller’s Jay: AZ, CA, CO, ID, MT, NM, NV, OR, UT, WA, WY.
- Pileated Woodpecker: AL, AR, CA, FL, GA, IA, ID, IL, IN, KS, KY, LA, MA, ME, MI, MN, MO, MS, MT, NV, ND, NH, NY, OH, OK, OR, PA, SC, TN, TX, VA, VT, WA, WI, WV.

Note that we consider all eBird grid cells, regardless of whether the species was detected there or not. Let n be the total number of grid cells considered for a species. For each cell, we consider all checklists occurring at the location at any time of the year (thus, both in breeding and non-breeding seasons). For cluster location $m = 1, \ldots, n$, let N_m be the number of checklists at the location, and let M_m the total number

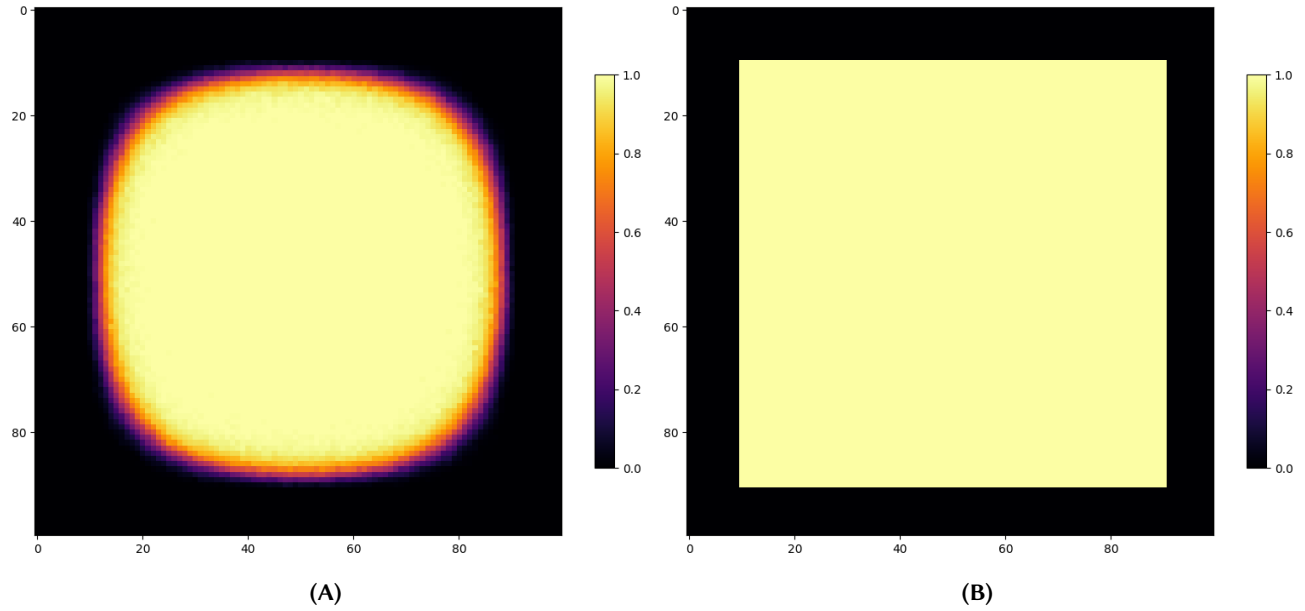

Supp. Figure S2. Repopulation from a centrally located pixel in a habitat region. The repopulation occurs for $n = 40$ rounds. (A): Standard computation with coin toss. (B): Computation with no coin toss.

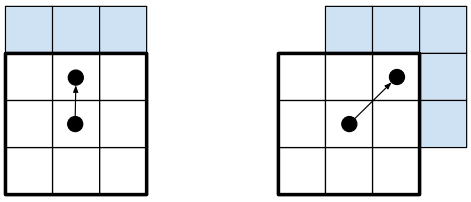

Supp. Figure S3. Diagonal propagation gives access to 5 pixels not previously directly reachable, compared to 3 pixels for edge-adjacent propagation.

of individuals of a species seen at the location (summed over all location checklists); thus, $F_m = M_m/N_m$ is the average number of birds/checklist detected at the cluster location.

For each cluster location, we selected the 3×3 land cover pixels centered on the grid cell; these pixels cover an area of about 900×900 meters, roughly comparable with the area that may be covered in a checklist of length < 2 km. In total, for n cluster locations, $9n$ pixels will be selected. For a pixel $k = 1, 2, \ldots, 9n$, let L_k be the land cover type of the pixel, and let $loc(k) \in \{1, \ldots, n\}$ be the grid cell associated with the pixel. Let $b_k = F_{loc(k)}$ be the average number of individuals of a focal species per checklist reported at the location corresponding to pixel k.

For land cover type i, we let $B_i = \text{Avg}\{b_k \mid L_k = i, k = 1, \ldots, 9n\}$ be the average sightings per checklist in pixels of land cover type i. Let $B_F = \max\{B_i \mid i \textit{ is a habitat or forest land cover}\}$ be the maximum sightings frequency in habitat or forest land cover. For non-forest, non-habitat land covers i, we compute the permeability $\hat{p}_i$ via

$$\hat{p}_i = \max\big(\tilde{p}_i, \min(1, B_i/B_F)\big) \ .$$

Above, the max ensures that $\hat{p}_i \geq \tilde{p}_i$; the min ensures that $\hat{p}_i \leq 1$. Supp. Table S1 reports the resulting permeability values for all IUCN land cover classes with permeability greater than 0.01. All these permeability values are derived for 1 km; we convert them to the pixel size of 300m via $p_i = \hat{p}_i^{0.3}$, for every land cover type i.

S2 Validation Methods

S2.1 Preparing eBird and Connectivity Data

We extracted all eBird checklists for the US states under consideration. We then applied eBird practices [Johnston et al.(2021)] to filter the eBird checklists down to those with relatively constrained effort i.e., those that were "complete", with "stationary" or "traveling" protocols, distances under 2 km, and durations between 10 minutes and 5 hours, and <10 observers. In addition, we considered checklists only during the breeding season (April-June for Acorn Woodpecker, and May-June for Pileated Woodpecker and Steller's Jay), because we expect this to be the time of year when individuals are least likely to disperse [Rushing et al.(2015), Greenwood and Harvey(1982)], and so their abundance reflects a state in between dispersal events.

We clustered the eBird checklists into *grid cells* according to a grid with resolution 0.01 degrees of latitude and longitude. Each grid cell corresponds to an area of about 1 km^2, which is an approximate match for our checklist

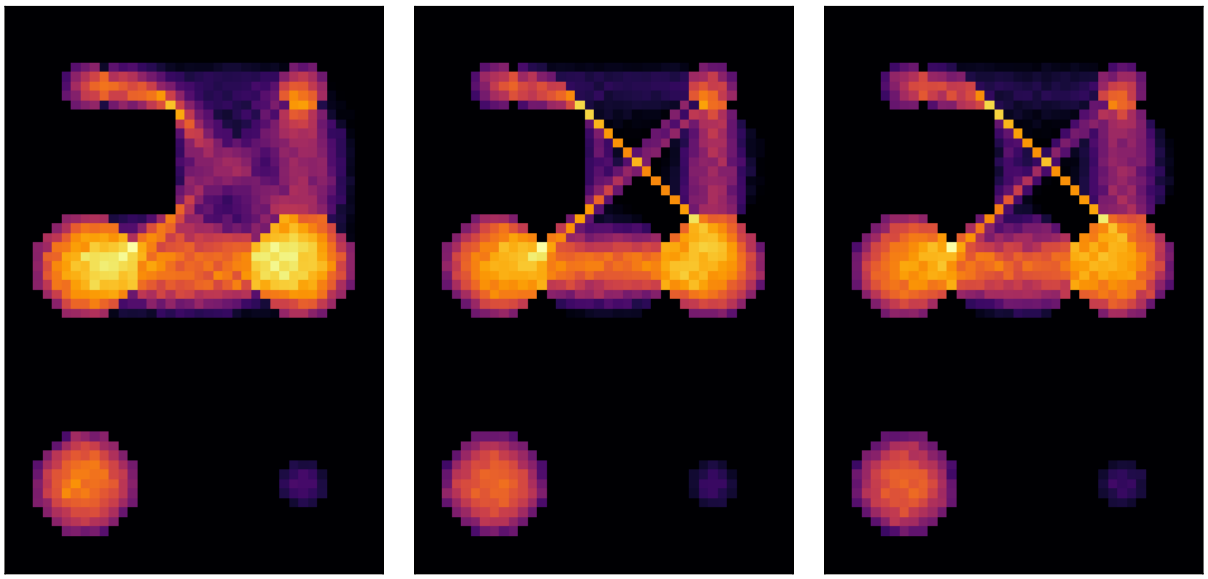

(A) (B) (C)

Supp. Figure S4. EcoScape flow layer produced by the artificial landscape described in Section 2.1.5. (A): Standard computation: coin toss and update threshold of 0.05. (B): Coin toss, and update threshold of 0. (C): No coin toss, update threshold of 0.05.

length upper-bound of 2 km (during a checklist, observers are unlikely to travel in straight lines).

Next, we filtered down the grid cells to only those with at least 10 checklists to retain only those cells with a minimum amount of eBirding effort. For each grid cell, we calculated the total number of checklists, the average distance of those checklists (where "stationary" checklists had a distance of 0 km) and the average duration of the checklists. For each cell we considered all checklists that counted the focal species (i.e., those that did not use an "X" as a count). We then calculated the *local abundance* of the species in each grid cell as the sum of checklist counts in that cell. We acknowledge that this is not a true measure of abundance, but a proxy for it. In addition, as we would expect total counts to increase linearly with the number of checklists, we accounted for this in our validation models (see below) and by performing sensitivity analyses (Supplementary Information S3.5).

For each grid cell of checklists, we considered the 3×3 raster pixels of habitat connectivity underlying the cell. We determined that the cell occurs in the species' habitat if at least one of the nine pixels is in the habitat, and we associated with each cell the average connectivity across pixels.

A natural question in habitat connectivity modeling is whether the association between connectivity and abudance can be better explained by connectivity than by habitat patch size *per se*, given the primacy of patch area in ecology [Manning et al.(2006), Wintle et al.(2019), Lomolino(2000), La Sorte et al.(2020)]. In other words, does connectivity predict abundance beyond area effects? We therefore calculated the area (km^2) of the forest patch to which each grid cell belongs. We log-transformed patch size given the wide range of sizes (from single-pixel, 0.09 km^2 patches, to patches > 50,000 km^2) and the uneven size distribution (very many small patches, but only a handful of large ones).

S2.2 Validation Modeling

In the first model—the *effort-only model*—local abundance was modeled as a function of total checklists, average checklist distance, and average checklist duration, all of which were log-transformed. These effort covariates allow for the fact that counts are expected to increase with the number of checklists as well as the average distance and duration of those checklists.

In the second model—the *area model*—we included (log) patch area in addition to effort to test the assumption that local abundance increases with patch area. This model can be thought of as the most important benchmark for comparison whether connectivity explain abundance better than simple area effects.

In the third model— the *connectivity model*—the area covariate is replaced with the average connectivity (again retaining the effort covariates).

In the fourth model—the *full model*—we included both patch area and a measure of *relative connectivity*. For all three species, average connectivity across cells was strongly positively correlated with (log) patch area (ρ = 0.82-0.86) and so we would face issues of multicollinearity in the model

Code	Landcover Name	ACWO	STJA	PIWO
0	—	0.000	0.519	0.407
100	1. Forest	1.000	1.000	1.000
101	1.1. Forest – Boreal	1.000	1.000	1.000
104	1.4. Forest – Temperate	1.000	1.000	1.000
105	1.5. Forest – Subtropical/tropical dry	1.000	1.000	1.000
106	1.6. Forest – Subtropical/tropical moist lowland	1.000	1.000	1.000
107	1.7. Forest – Subtropical/tropical mangrove	1.000	1.000	1.000
108	1.8. Forest – Subtropical/tropical swamp	1.000	1.000	1.000
109	1.9. Forest – Subtropical/tropical moist montane	1.000	1.000	1.000
201	2.1. Savanna - Dry	0.373	0.116	0.421
202	2.2. Savanna - Moist	0.000	0.000	0.570
300	3. Shrubland	0.000	0.000	0.455
303	3.3. Shrubland – Boreal	0.000	0.596	0.465
304	3.4. Shrubland –Temperate	0.643	0.825	0.683
305	3.5. Shrubland – Subtropical/tropical dry	0.418	0.405	0.307
306	3.6. Shrubland – Subtropical/tropical moist	0.000	0.000	0.759
307	3.7. Shrubland – Subtropical/tropical high altitude	0.777	0.899	0.000
308	3.8. Shrubland – Mediterranean-type shrubby vegetation	1.000	0.790	0.382
401	4.1. Grassland – Tundra	0.162	0.733	0.368
404	4.4. Grassland – Temperate	0.969	0.395	0.483
405	4.5. Grassland – Subtropical/tropical dry	0.969	0.258	0.111
406	4.6. Grassland – Subtropical/tropical seasonally wet/flooded	0.000	0.000	0.586
500	5. Wetlands (inland)	0.459	0.527	0.666
501	5.1. Wetlands (inland) – Permanent rivers/streams/creeks	0.272	0.569	0.969
502	5.2. Wetlands (inland) – Seasonal/intermittent/irregular rivers	0.285	0.481	0.734
505	5.5. Wetlands (inland) – Permanent freshwater lakes (over 8 ha)	0.579	0.643	0.725
506	5.6. Wetlands (inland) – Seasonal/intermittent freshwater lakes (over 8 ha)	0.643	0.551	0.689
507	5.7. Wetlands (inland) – Permanent freshwater marshes/pools (under 8 ha)	0.000	0.000	0.751
510	5.10. Wetlands (inland) – Tundra wetlands	0.000	0.674	0.489
511	5.11. Wetlands (inland) – Alpine wetlands	0.329	0.781	0.693
513	5.13. Wetlands (inland) – Permanent inland deltas	0.323	0.574	0.701
515	5.15. Wetlands (inland) – Seasonal/intermittent saline, brackish or alkaline	0.000	0.454	0.615
600	6. Rocky Areas (e.g., inland cliffs, mountain peaks)	0.174	0.523	0.252
801	8.1. Desert – Hot	0.071	0.014	0.000
802	8.2. Desert – Temperate	0.091	0.200	0.000
803	8.3. Desert – Cold	0.168	0.342	0.109
900	9. Marine Neritic	0.323	0.555	0.459
908	—	0.000	0.000	0.309
909	9.9 Seagrass (Submerged)	0.230	0.490	0.457
1200	12 Marine Intertidal	0.168	0.576	0.465
1206	12.6 Tidepools	0.251	0.472	0.381
1207	12.7 Mangrove Submerged Roots	0.000	0.000	1.000
1401	14.1 Arable Land	0.498	0.380	0.542
1402	14.2 Pastureland	0.969	0.600	0.548
1403	14.3 Plantations	0.619	0.855	0.810
1404	14.4 Rural Gardens	0.000	0.969	0.969
1405	14.5 Urban Areas	0.553	0.516	0.529

Supp. Table S1. IUCN land cover codes, classes and their permeability for Acorn Woodpecker (ACWO), Steller's Jay (STJA), and Pileated Woodpecker (PIWO). All land cover classes with permeability greater than 0.01 for at least a species are listed.

were we to include both covariates. We thus calculated *relative connectivity* by extracting the residuals from a linear model of connectivity against (log) patch area, and included both patch area and relative connectivity in the model. Thus, this model accounts for both the area of the forest patch but also the relative connectivity, given the area. All covariates were scaled have a mean of 0 and standard deviation of 1. Finally, we included an intercept-only *null model*.

We ran all five models, calculating ΔAIC values and model weights, and ranking the models accordingly. We considered and evaluated all models within 2 ΔAIC. For each covariate retained in the model we extracted the covariate coefficient, associated standard error, and test statistics.

S3 Sensitivity Analyses

S3.1 Output Stability

The connectivity and flow layers are computed as the average of randomized simulations, and are thus affected by random fluctuations. To characterize the precision of the results, we need to measure the standard deviation of such fluctuations. To do so, we considered the distributions of Acorn Woodpecker in Oregon and Pileated Woodpecker in North Carolina. We chose these states for the diversity of their forest land cover, which consists of large patches in Oregon, and a mix of large patches and finely dispersed patches along riparian corridors in North Carolina. We computed the connectivity and flow layers 100 times, using the average of 100 simulations in each computation; we then measured the standard deviation of the values computed at each pixel. The remainder of the results presented in the paper are computed using 1,000 simulations, thereby having less uncertainty (the standard deviation is reduced by $\sqrt{10}$).

Our analysis of output stability using 100 simulations indicated that the standard deviation of the computed connectivity layer exceeded 0.05 for fewer than 1% of the pixels. To perform this analysis, we grouped locations into connectivity intervals 0.1 wide and our results indicated that 100 simulations would have been sufficient to obtain accurate results.

S3.2 Fixed vs Half-Cauchy Dispersal

When using EcoScape on our three focal species we drew n from a half-Cauchy distribution. However, it is computationally more simple to fix n as $n = d$. We therefore recalculated connectivity values across the contiguous US for our three focal species. We found that connectivity based on fixed dispersal resulted in much faster computation times (Supp. Table S2) and were highly correlated with connectivity based on the half-Cauchy (ρ = 0.990–0.992).

We then compared our main *connectivity model* with a *fixed dispersal model* model, and found the latter to perform slightly worse for Acorn Woodpecker (ΔAIC = 0.85), and worse for Pileated Woodpecker (ΔAIC = 30.35) and Steller's Jay (ΔAIC = 4.46). Thus, using the half-Cauchy would be ideal if unlimited by computation times but, for efficiency over large spatial scales and many species, users may prefer to use fixed dispersal distances.

S3.3 Varying Dispersal Distance

In EcoScape, the number of propagation rounds, n, is equal to (or drawn from a half-Cauchy based on) d. However, we were interested in validating whether EcoScape connectivity estimates would depend on the relative value of d. We therefore re-computed connectivity values for our three focal species where $n = 2d$ and $n = 0.5d$. Our original connectivity values were highly correlated with the $2d$ (ρ = 0.972–0.984) and $0.5d$ (ρ = 0.982–0.986) values. These results show that EcoScape is fairly robust to uncertainty in dispersal distance estimates.

We then constructed validation models identical to the connectivity model but using these alternate permutations and compared them to the main model. We found that both the *double-dispersal model* (ΔAIC = 1.25) and the *half-dispersal model* (ΔAIC = 1.25) performed slightly worse for Acorn Woodpecker. For both Pileated Woodpecker and Steller's Jay, the half-dispersal model performed better (PIWO:ΔAIC = -71.02; STJA: ΔAIC = -3.56) but the double-dispersal model performed worse (ΔAIC = 59.59; STJA: ΔAIC = 10.88).

S3.4 No permeability

To validate our model of dispersal and landscape matrix permeability, we repeated the connectivity computation but setting the permeability to 0 everywhere outside the habitat. In this way, locations can be repopulated only from locations within the same patch. To quantify the benefits of EcoScape including landscape matrix permeability, we compared a *no permeability model* with the connectivity model. We found the no permeability model to generally perform much worse than the connectivity model (ACWO: ΔAIC = 8.97; PIWO: ΔAIC = 33.08; STJA: ΔAIC = 10.49), indicating that including the permeability layer increased our ability to predict local abundance.

S3.5 Alternate Validation Response Variables

To assess whether the results of our validation models depended on the response variable used (i.e., local abundance of focal bird species), we calculated two alternate response variables for use in AIC-based multi-model inference.

First, we calculated *average abundance* as the total counts in a grid cell divided by the number of checklists in that cell. We modeled average abundance with negative-binomial GLMs using the same five models as our main model set, except excluding total checklists from the effort covariates. These models were ranked identically (Supp. Table S3) to those in the main validation analysis (Supp. Table 1).

Second, we calculated the proportion of checklists that contained the focal species. Unlike for the other response variables, here, we were able to include all checklists where the focal species was indicated with an "X". Thus, this variable is a measure of *occurrence probability* of a focal species on a checklist in a grid cell. We modeled occurrence probability in binomial GLMs with the same model structures as those for average abundance. Once again, the model rankings were identical (Supp. Table S4) and the weights similar to those in the main validation analysis.

S4 Comparison with Omniscape

Although EcoScape uses a completely different approach to mapping habitat connectivity than existing circuit- and

Flow?	Dispersal type	Tile n (px)	Border b (px)	Batch size	Time (s)	Speed (kpx/s)
No	half-Cauchy	5,000	180	25	1,544	193
No	fixed	5,000	45	25	1,267	235
Yes	half-Cauchy	500	180	1	20,882	14
Yes	fixed	1,000	45	5	3,561	84

Supp. Table S2. Computation parameters, times, and speeds, for EcoScape connectivity and flow computation. The speeds are expressed in kilopixels per second (kpx/s).

(A) Acorn Woodpecker

Model	Avg. distance	Avg. duration	Patch size	Avg. connect.	Rel. connect.	df	ΔAIC	Model weight
Connectivity	0.04	0.33	–	0.19	–	5	0	0.73
Full	0.04	0.33	0.14	–	0.12	6	1.95	0.27
Area	0.03	0.34	0.15	–	–	5	13.24	0.00
Effort-only	0.02	0.35	–	–	–	4	27.66	0.00
Null	–	–	–	–	–	2	123.91	0.00

(B) Pileated Woodpecker

Model	Avg. distance	Avg. duration	Patch size	Avg. connect.	Rel. connect.	df	ΔAIC	Model weight
Connectivity	0.06	0.38	–	0.25	–	5	0	0.71
Full	0.06	0.38	0.16	–	0.19	6	1.83	0.29
Area	0.05	0.41	0.18	–	–	5	58.23	0.00
Effort-only	0.04	0.42	–	–	–	4	101.69	0.00
Null	–	–	–	–	–	2	372.27	0.00

(C) Steller's Jay

Model	Avg. distance	Avg. duration	Patch size	Avg. connect.	Rel. connect.	df	ΔAIC	Model weight
Full	0.05	0.29	0.24	–	0.16	6	0	0.58
Connectivity	0.05	0.28	–	0.25	–	5	0.61	0.42
Area	0.03	0.32	0.21	–	–	5	37.93	0.00
Effort-only	0.02	0.32	–	–	–	4	87.50	0.00
Null	–	–	–	–	–	2	222.91	0.00

Supp. Table S3. AIC-based multi-model comparison of the predictors of average abundance in three focal bird species. Average abundance was modeled in a negative-binomial GLM as a function of combinations of covariates including eBird effort, habitat patch size, and habitat connectivity. Local abundance was summed across eBird checklists in a grid cell and then divided by the number of checklists in that cell. Avg. distance is the average checklist distance; Avg. duration is the average checklist duration; Patch size is the size of the habitat patch to which that cell belongs; Avg. connect. is the average habitat connectivity across the cell; Rel. connect. is the relative habitat connectivity after controlling for patch size; df is the model degrees of freedom; ΔAIC is the difference in AIC between each model and the top-ranked model.

graph-based models, we chose to compare its outputs, efficiency, and validation with the leading connectivity algorithm, Omniscape [Landau et al.(2021)] to ensure that EcoScape's outputs are in line with predicted by Omniscape. We used Omniscape to calculate *cumulative current* for our three focal species across the US states in their ranges. We then compared the computation time of Omniscape with EcoScape, as well as the predictive power of cumulative current vs. EcoScape's connectivity, with respect to eBird counts for the species.

Omniscape models a landscape matrix via a raster in which every pixel ij has a given electrical conductance G_{ij}, where conductance is the reciprocal of resistance. For each habitat pixel, Omniscape considers a circular region around that pixel, and computes the total current that can flow to the

(A) Acorn Woodpecker

Model	Avg. distance	Avg. duration	Patch size	Avg. connect.	Rel. connect.	df	ΔAIC	Model weight
Connectivity	0.00	0.29	–	0.20	–	4	0	0.58
Full	0.00	0.29	0.19	–	0.10	5	1.00	0.35
Area	0.00	0.30	0.19	–	–	4	4.08	0.07
Effort-only	-0.02	0.31	–	–	–	3	17.60	0.00
Null	–	–	–	–	–	1	54.94	0.00

(B) Pileated Woodpecker

Model	Avg. distance	Avg. duration	Patch size	Avg. connect.	Rel. connect.	df	ΔAIC	Model weight
Connectivity	0.06	0.42	–	0.30	–	4	0	0.74
Full	0.06	0.42	0.21	–	0.22	5	2.14	0.26
Area	0.05	0.45	0.23	–	–	4	38.62	0.00
Effort-only	0.03	0.47	–	–	–	3	59.87	0.00
Null	–	–	–	–	–	1	259.77	0.00

(C) Steller's Jay

Model	Avg. distance	Avg. duration	Patch size	Avg. connect.	Rel. connect.	df	ΔAIC	Model weight
Full	0.02	0.31	0.30	–	0.19	5	0	0.89
Connectivity	0.03	0.30	–	0.34	–	4	4.15	0.11
Area	0.00	0.34	0.31	–	–	4	23.52	0.00
Effort-only	-0.02	0.35	–	–	–	3	74.54	0.00
Null	–	–	–	–	–	1	165.08	0.00

Supp. Table S4. AIC-based multi-model comparison of the predictors of occurrence in three focal bird species. Proportion of occurrences was modeled in a binomial GLM as a function of combinations of covariates including eBird effort, habitat patch size, and habitat connectivity. Proportion of occurrences was calculated by dividing the number of eBird checklists recording at least one individual of a focal species in a grid cell by the total number of checklists in that cell. Avg. distance is the average checklist distance; Avg. duration is the average checklist duration; Patch size is the size of the habitat patch to which that cell belongs; Avg. connect. is the average habitat connectivity across the cell; Rel. connect. is the relative habitat connectivity after controlling for patch size; df is the model degrees of freedom; ΔAIC is the difference in AIC between each model and the top-ranked model.

selected pixel from other habitat pixels in the region. This quantity—*cumulative current*—is similar to EcoScape's connectivity when considered inside the habitat, while it is more similar to EcoScape's flow when considered outside of the habitat, but we note that OmniScape produces only one output type where EcoScape produces two. To allow for a comparison between EcoScape and Omniscape outputs, we took the radius of Omniscape's circular regions to be equal to the dispersal distance used in EcoScape.

Omniscape takes as input a conductance layer, which corresponds to EcoScape's permeability. As the conductance must be strictly greater than zero, we prepared the Omniscape input conductance raster G via $G_{ij} = 1 + 10 \cdot p_{ij}$, where p is the EcoScape permeability layer. This ensured non-zero conductance while closely preserving EcoScape's permeability. As current source region, we used the habitat. Further, we used the dispersal distance as the radius of the circular region.

S4.1 Computation Times

Omniscape and EcoScape take advantage of different computation hardware: Omniscape relies on CPU computation, and benefits from multiple CPU cores, while EcoScape relies on GPU computation, and benefits from multi-core GPUs. To compare the computational speed of the two frameworks, we chose a computational platform that is easily available, and that provides a large number of both CPU and GPU cores: a MacBook Pro M4 with 16 CPU cores (12 performance cores and 4 efficiency cores) and 40 GPU cores. The comparison is also fair from an energy point of view: both CPU cores and GPU cores use about 35 W of electrical power, and, among chips with the same silicon process technology, electrical power is closely related to computational power.

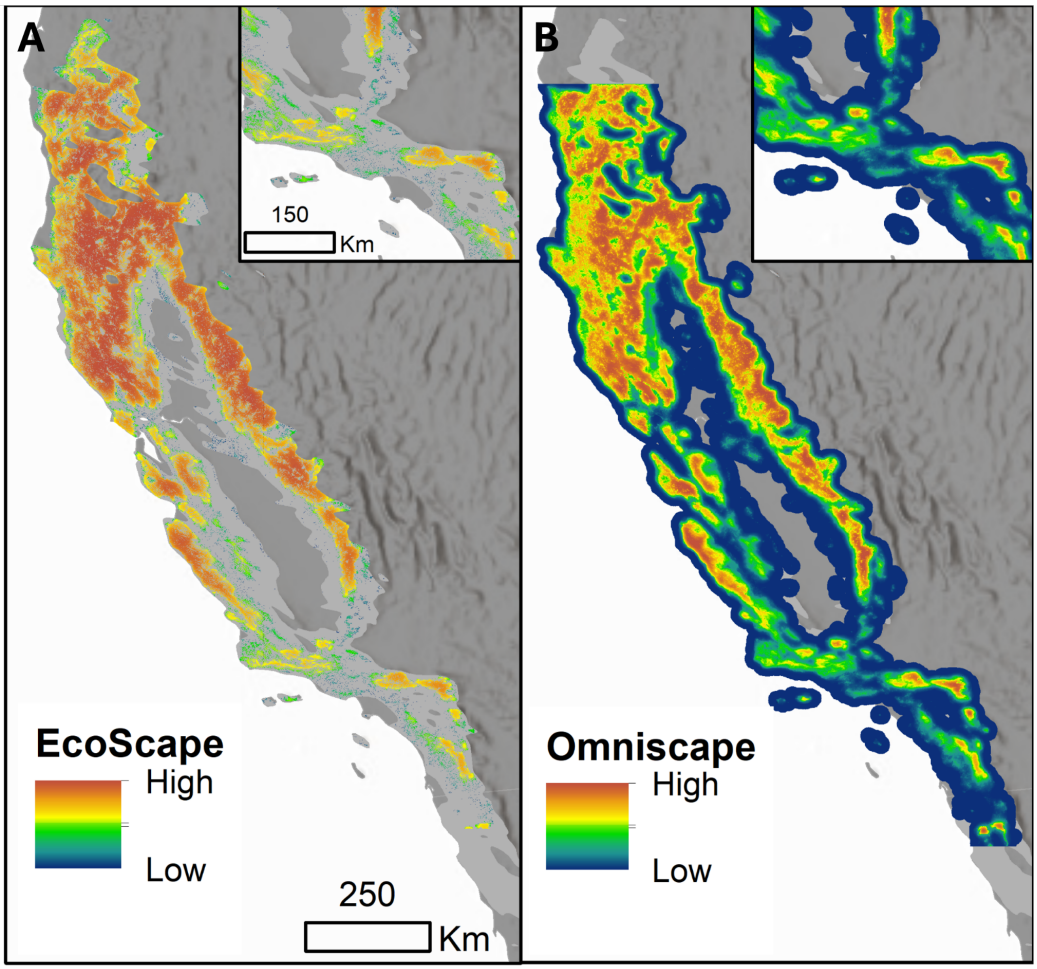

Supp. Figure S5. Habitat connectivity layers for Acorn Woodpecker scaled for the Ecoscape (A) and Omniscape (B) algorithms.

We compared the running times required for computing habitat connectivity (EcoScape) and cumulative current (Omniscape) for the three sample species across their US range. We ran Omniscape with 12 threads, matching the number of performance CPU cores, which were fully utilized. In Omniscape, to speed up the computation, it is common to divide the raster into blocks, and consider as current sources only the center pixel of each block. Thus, we used 3×3 blocks, so 1 in 9 pixels is considered a source. We selected a number m of EcoScape simulations that replicates the Omniscape seed sampling density of 1 pixel every 3×3 block. Since each EcoScape simulation selects as a seed 4 pixels every $(2d+1)^2$ pixels, where d is the dispersal distance, to replicate the Omniscape sampling density we needed $n = (2d+1)^2/36$ simulations. For EcoScape, we used 500×500 tiles and a batch size of 20.

For each species in every US state within its range, we calculated the computation times for EcoScape and Omniscape, as well as the *speedup* i.e., the number of times faster EcoScape was (Supp. Table S5).

On the MacBook Pro M4 MAX, with our specified settings, Omniscape took 18,482.1 seconds to process the three species in all the US states within their distribution (297,986,556 pixels in total), while EcoScape takes 506.5 seconds. The average speedup provided by EcoScape is thus 36.5. The speedup varies across states: for example, for Pileated Woodpecker, the speedup goes from a low of 7.1 for North Dakota, to a high of 62 in Georgia. The difference in speedup can be attributed to differentials in the distribution of habitat among states. In

Species	State	Omniscape (s)	EcoScape (s)	Speedup
ACWO	US-NM	53.00	11.39	4.65
ACWO	US-AZ	81.32	16.32	4.98
ACWO	US-NV	55.14	9.43	5.85
ACWO	US-OR	40.53	6.41	6.33
PIWO	US-ND	35.94	5.02	7.16
ACWO	US-CA	247.56	25.13	9.85
PIWO	US-CA	294.75	15.69	18.79
STJA	US-AZ	33.68	1.74	19.39
PIWO	US-IA	203.33	10.05	20.22
PIWO	US-KS	127.77	6.22	20.54
STJA	US-NV	46.46	2.16	21.54
PIWO	US-FL	375.86	14.81	25.37
PIWO	US-OR	391.95	14.91	26.28
STJA	US-CA	106.79	4.05	26.40
PIWO	US-OK	268.34	8.86	30.30
PIWO	US-TX	649.97	20.34	31.96
PIWO	US-MT	352.37	10.88	32.39
PIWO	US-WI	493.04	14.57	33.84
STJA	US-UT	54.30	1.60	34.03
PIWO	US-WA	441.32	12.24	36.05
STJA	US-NM	58.60	1.59	36.93
PIWO	US-MO	582.97	15.74	37.03
PIWO	US-IL	510.10	13.60	37.50
PIWO	US-MI	881.20	22.24	39.63
PIWO	US-IN	327.86	8.25	39.73
PIWO	US-MN	711.39	17.71	40.17
PIWO	US-ID	545.97	13.37	40.83
PIWO	US-MA	186.11	4.53	41.12
PIWO	US-OH	421.37	9.81	42.97
PIWO	US-SC	457.85	10.08	45.42
PIWO	US-LA	569.97	12.41	45.95
PIWO	US-MS	529.78	11.51	46.02
PIWO	US-KY	608.53	13.01	46.76
PIWO	US-AL	550.93	11.53	47.79
STJA	US-WY	58.45	1.22	47.84
PIWO	US-AR	542.34	11.25	48.22
PIWO	US-PA	493.82	10.17	48.54
STJA	US-CO	73.11	1.43	51.04
PIWO	US-VA	751.22	14.44	52.04
PIWO	US-VT	233.59	4.43	52.76
PIWO	US-NH	240.00	4.54	52.82
PIWO	US-NC	726.87	13.68	53.15
PIWO	US-TN	596.63	11.09	53.82
PIWO	US-ME	519.45	9.62	53.99
PIWO	US-NY	896.45	16.48	54.39
PIWO	US-WV	606.81	10.03	60.50
PIWO	US-GA	854.69	13.61	62.81
STJA	US-OR	140.39	1.97	71.25
STJA	US-ID	161.55	2.18	74.03
STJA	US-MT	139.31	1.68	83.08
STJA	US-WA	151.40	1.52	99.84

Supp. Table S5. Computation times for EcoScape and Omniscape in each state within the species' range. The times are listed in increasing order of speedup offered by EcoScape.

states where habitat (i.e., forest) is widely distributed, such as North Carolina and New York, both EcoScape and Omniscape must process all pixels, and the speedup is about 60. In states where habitat is more sparse, such as California, where wide portions of the state are far from forests, Omniscape can skip any pixel that is not within dispersal distance (45 pixels or less, in our case) from habitat. In contrast, EcoScape can only skip computation when an entire tile of 500×500 pixels contains no habitat. Thus, in states where the habitat is sparse, Omniscape can skip computation for

more pixels than EcoScape, and the relative speed gain of EcoScape decreases.

EcoScape can also take advantage of NVidia GPUs, which can be conveniently rented on the Cloud, or obtained via Google Colab. Using an A100 NVidia GPU, EcoScape can complete the computation in 280 seconds, bringing the speedup to 66.

S4.2 Validation Model Comparison with EcoScape

Across forested grid cells, average cumulative current estimates from Omniscape were highly correlated with average connectivity values from EcoScape for all three species (ACWO: ρ = 0.894, PIWO: ρ = 0.914, STJA: ρ = 0.923).

For each species we constructed a model identical in structure to the *connectivity model* but replacing the total connected pixels with Omniscape-derived cumulative current. These models were compared to the rest of the model set using AIC. For all three species we found that the *Omniscape model* performed less well than the connectivity model (ACWO: ΔAIC = 0.73, weight = 0.33; PIWO: ΔAIC = 75.25, weight < 0.01; STJA: ΔAIC = 3.51, weight 0.11), indicating that, for these three species, connectivity values derived from EcoScape were generally better at predicting local abundance than Omniscape's cumulative current.